PAPER

Check for updates

From chemistry to targeted cancer therapy: potent benzimidazole-1,2,3-triazole hybrid-loaded nanogels against breast and colorectal malignancies

Azizah M. Malebari,[a] Mohamed A. M. Ali, [iD][b] Arafa Musa, [iD]*[c] Magdi E. A. Zaki,[d] Sobhi M. Gomha, [iD][e] Moataz A. Soliman,[f] Mohamed A. Abdelgawad,[g] Della Grace Thomas Parambi,[g] Mohamed R. Aouad,[h] Hamada S. Abulkhair [iD][ij] and Hany E. A. Ahmed [iD]*[i]

The therapeutic limitations of conventional anticancer agents, particularly in treating mucosal and epithelial malignancies such as breast and colorectal cancers, necessitate the development of advanced drug delivery systems. This study explores the integration of benzimidazole-1,2,3-triazole hybrids into chitosan/polyvinyl pyrrolidone nanogels to enhance pharmacological performance and target specificity. Comprehensive physicochemical characterization confirmed successful encapsulation and favorable nanogel properties, including controlled particle size, stability, and morphology. Among the tested formulations, the **12ng** nanogel demonstrated superior cytotoxicity against the epithelial cancer cells, MDA-MB-231 (IC_{50} = 3.13 ± 0.22) and Caco-2 (IC_{50} = 3.64 ± 0.25) μM, surpassing the reference drug staurosporin. Enzymatic assays revealed potent inhibition of topoisomerase I and II, as well as tubulin polymerization. Flow cytometry and apoptosis analysis confirmed G0/G1 cell cycle arrest and late-stage apoptosis induction. Molecular docking studies supported the strong binding affinity (-9.50 kcal mol^{-1}) of **12ng** to topoisomerase I, validating its' multitarget mechanism. These findings underscore the potential of nanogel-delivered benzimidazole-1,2,3-triazole hybrids as promising candidates for targeted cancer therapy.

[a]Department of Pharmaceutical Chemistry, Faculty of Pharmacy, King Abdulaziz University, Alsulaymanyah, Jeddah 21589, Saudi Arabia

[b]Department of Biology, College of Science, Imam Mohammad Ibn Saud Islamic University (IMSIU), Riyadh 11623, Saudi Arabia

[c]Department of Pharmacognosy, College of Pharmacy, Jouf University, Sakaka, Aljouf 72388, Saudi Arabia. E-mail: akmusa@ju.edu.sa

[d]Department of Chemistry, Faculty of Science, Imam Mohammad Ibn Saud Islamic University (IMSIU), Riyadh 11623, Saudi Arabia

[e]Chemistry, Faculty of Science, Islamic University of Madinah, Madinah, 42351, Saudi Arabia

[f]Deanship of Preparatory Year, Prince Sattam Bin Abdulaziz University, Al-Kharj 16273, Saudi Arabia

[g]Department of Pharmaceutical Chemistry, College of Pharmacy, Jouf University, Sakaka, Aljouf 72388, Saudi Arabia

[h]Department of Chemistry, Faculty of Sciences, Taibah University, Al-Madina Al-Munawarah 30002, Saudi Arabia

[i]Pharmaceutical Organic Chemistry Department, Faculty of Pharmacy, Al-Azhar University, Nasr City 11884, Cairo, Egypt. E-mail: heahmad@azhar.edu.eg

[j]Pharmaceutical Chemistry Department, Faculty of Pharmacy, Horus University, International Coastal Road, New Damietta 34518, Egypt

1 Introduction

Breast cancer remains a growing global threat. In women, it remains the most frequently diagnosed malignancy (11.60% of all cancers).[1,2] It is the second most prevalent cancer worldwide, causing ~670 thousand deaths each year.[1] This figure reflects a persistent and growing burden. By 2050, 3.2 million new cases and 1.10 million deaths are expected each year.[3] Colorectal cancer represents another major global health challenge, ranking among the top causes of cancer-related morbidity and mortality worldwide.[4,5] Its increasing incidence, particularly in younger populations, highlights the urgent need for improved therapeutic strategies. While considerable advancements have been achieved in the pharmacological management of breast and colorectal cancers, the field remains in critical need of further innovation. Existing chemotherapeutics are frequently hindered by limitations such as the emergence of drug resistance,[6] inadequate efficacy in treating aggressive or metastatic subtypes,[7] and adverse toxicity profiles.[8] These limitations underscore the urgent need for continued research to discover novel, targeted, and more tolerable therapies to enhance clinical outcomes and bridge the existing gap in care. To address

Table 1 Advantages of CPPNs over traditional nanogels

Feature	Chitosan/PVP nanogels (CPPNs)	Traditional nanogels (*e.g.*, PEG, PLGA)
Biocompatibility	Both chitosan and PVP are FDA-approved and non-toxic	PEG is biocompatible, but PLGA may cause acidic degradation byproducts
Mucosal adhesiveness	Strong mucoadhesive properties due to chitosan, enhancing retention at mucosal sites	PEG and PLGA lack intrinsic mucosal adhesiveness
Mechanical stability	PVP enhances structural integrity and elasticity of the nanogel matrix	Requires crosslinkers or additives to improve mechanical strength
Controlled drug release	Dual polymer system allows fine-tuning of release kinetics *via* pH and temperature	Release profiles are often less tunable without complex modifications
Formulation flexibility	Can be fabricated as hydrogels, nanogels, or nanofibers with diverse drug loading strategies	Some systems (*e.g.*, alginate) are limited by gelation conditions or drug compatibility
Targeting potential	Chitosan can be functionalized with ligands for active targeting	Targeting often requires external conjugation or surface modification
Environmental responsiveness	Responsive to pH and temperature changes, suitable for tumor microenvironment targeting	Responsiveness depends on polymer type; often requires additional design complexity

this gap, scientific research should prioritize uncovering the mechanism of resistance and improving the drug delivery systems, such as nanocarriers,[9,10] to enhance efficacy and reduce systemic toxicity. In this context, nanogel formulations offer promising advantages over traditional delivery systems. These advantages include enhanced drug stability, controlled release, and improved tumor-targeting capabilities,[9–11] which collectively may reduce toxicity and increase therapeutic efficacy.[9,12] The relatively high-water contents, small size (20–200 nm), high drug-loading capacity, and tunable degradation and rheological properties of nanogel formulations allow for controlled and sustained drug release,[13] improved tumor penetration,[14] and reduced systemic toxicity.[9] These features make nanogels a promising strategy to enhance therapeutic precision and to minimize off-target effects in breast and colon cancer therapy.[15] Nanogels can be tailored to respond to tumor-specific conditions such as pH changes,[16] redox potential,[15] and temperature.[16]

The incorporation of specific heterocycles or functional groups (*e.g.*, 1,2,4-triazole, amide, and sugar moieties) allows direct drug conjugation,[17,18] stability enhancement,[19] and intelligent release mechanisms tailored to tumor microenvironments.[9,11] In preclinical models, nanogel-based therapies have shown improved antitumor efficacy,[15] reduced systemic toxicity,[20] and potential for customized medicine,[21] especially in genetically diverse breast cancer subtypes.[15,22]

Chitosan/polyvinyl pyrrolidone nanogels represent a promising class of biomaterials[13,23] designed for advanced drug delivery in cancer therapy,[23] including breast and colorectal cancer.[15,22] Chitosan-based systems, including stimuli-responsive hydrogels and nanofibers, show promising selective activity against MDA-MB-231 and Caco-2 cancer cell lines.[24,25] The combination of chitosan with polyvinyl pyrrolidone enhances mechanical properties and biocompatibility, making chitosan/polyvinyl pyrrolidone nanogels (CPPNs) a viable platform for promising targeted delivery research.[22,26,27] This class of nanogels combines the biocompatibility and biodegradability of chitosan, a natural polysaccharide, with the mechanical stability and film-forming properties of polyvinyl

pyrrolidone (PVP), a synthetic polymer. The resulting hydrogel matrix offers a versatile platform for encapsulating and delivering therapeutic agents with high precision. Compared to other common types of nanogels, CPPNs have many advantages, especially in targeting mucosal and epithelial cancers[28] like colorectal and breast cancer (Table 1). These include, biocompatibility,[29] safety,[30] controlled pH-responsive release,[31] high drug loading efficiency,[32] and targeted drug delivery.[15,22,27] CPPNs can be designed to respond to pH changes,[31] enabling site-specific drug release and minimizing systemic side effects.[15,22,27] The porous and hydrated structure of the nanogel allows for efficient encapsulation of hydrophobic and hydrophilic drugs.[30,32] Crosslinking between chitosan and PVP improves the physical and chemical stability of CPPNs, ensuring sustained therapeutic effects.[28] CPPNs have shown potential in delivering chemotherapeutics to mucosal and epithelial cancers like colon and breast cancer cells,[26,28] enhancing cytotoxicity while sparing healthy tissue. These nanogels can be used to co-deliver agents targeting multiple pathways[26,33] (*e.g.*, topoisomerases and tubulin), overcoming drug resistance[24] and improving therapeutic outcomes.

Recently, innovations in nanogel design have incorporated heterocyclic structures into the polymer backbone to enhance both physicochemical stability and biological performance.[34] Among these, benzimidazole and 1,2,3-triazole stand out as pharmacologically significant scaffolds with broad therapeutic relevance.[35–37]

Benzimidazole functions as a purine analog with a wide range of bioactivity including anticancer,[38–40] antimicrobial,[41–43] antiviral,[44,45] and anti-inflammatory properties.[46,47] 1,2,3-Triazole-incorporating molecules are known for their anticancer,[48–51] antiviral,[52] antioxidant,[53] and neuroprotective effects.[54] They also serve as a versatile linker in drug design, enhancing molecular stability and reducing toxicity.[36,52] Benzimidazole-1,2,3-triazole hybrids have shown synergistic effects beyond that of individual components.[55] The incorporation of this moiety into nanogels allows for targeted drug delivery or site-specific release,[56] particularly in cancerous tissues, due to their responsiveness to pH and redox

conditions.[15,16] These multifunctional nanogels can co-deliver chemotherapeutics and bioactive agents, offering dual-action therapies for complex diseases like breast cancer.[57]

Recent studies have demonstrated that nanogels incorporating benzimidazole and 1,2,3-triazole moieties (**1–4**) exhibit potent antiproliferative activity against MDA-MB-231 breast cancer cells,[35,40,58,59] particularly through inhibiting tubulin polymerization[58,60] and topoisomerase[35,59,61] and apoptosis induction. For instance, compound **1** (Fig. 1) demonstrated remarkable cytotoxic activity against MDA-MB-231 and MCF-7 breast cancer cells, with IC_{50} values of 2.02 μM and 3.03 μM, respectively.[62] Similarly, the benzimidazole-1,2,3-triazole hybrids **5–7** showed better cytotoxicity than 5-FU against MDA-MB-231 and MCF-7 breast cancer cells. Among these latter, compound **5** exhibited IC_{50} values of 1.80 μM and 2.90 μM, respectively, compared to 7.80 μM and 12.40 μM for 5-FU.[40] Compound **8** demonstrated remarkable cytotoxic activity against MCF-7 breast cancer cells, with an IC_{50} of 6.81 μM, while exhibiting minimal toxicity toward normal WI-38 cells, indicating a favorable selectivity profile (SI = 5.76). Compound **8** also exhibited exceptionally good inhibitory activity against topoisomerase II (IC_{50} = 2.52 μM) surpassing doxorubicin (IC_{50} = 3.62 μM).[59]

The benzimidazole-1,2,3-triazole hybrid **9** exhibited strong anticancer activity against MCF-7 breast cancer cells, while showing negligible toxicity toward normal BEAS-2B cells, indicating selective cytotoxicity.[58] Apoptotic effect of this compound was confirmed through Annexin V and JC-1 assays. Flow cytometry analysis showed dose-dependent cell cycle arrest at the G2/M phase. Mechanistic studies confirmed that **9** inhibits tubulin polymerization (IC_{50} = 5.65 μM) and interacts effectively with circulating tumor DNA, suggesting a dual mechanism involving microtubule disruption and DNA intercalation. This compound occupied the active pocket of α/β-tubulin (PDB ID: 3×10^{22}), forming several hydrogen bonds (HB) and hydrophobic interaction with key amino acid residues (Tyr224, Lys254, and Gly144). In this interaction pattern, the 1,2,3-triazole ring participated in the formation of HB hydrogen bond (Lys254) and six hydrophobic interactions (Pro173, Tyr 224, Asn249, Leu255, Met259, and Ala 316).[58]

Recent research efforts have explored the incorporation of heterocyclic pharmacophores into nanocarrier systems to enhance anticancer efficacy and overcome multidrug resistance. Several studies have reported the design and synthesis of benzimidazole-1,2,3-triazole hybrids as potent multitarget inhibitors. For instance, Laxmikeshav *et al.* demonstrated that triazolo-linked benzimidazoles inhibit tubulin polymerization and induce cell cycle arrest in breast cancer cells, showing IC_{50} values in the low micromolar range.[58] Similarly, Othman *et al.* reported benzimidazole–triazole conjugates with strong

Ar	MDA-MB-231	MCF-7
1 p-Tolyl	2.02 μM	3.03 μM
2 4-F-Phenyl	3.08 μM	3.13 μM
3 3,5-Cl$_2$-Phenyl	5.02 μM	4.08 μM
4 3,5-(OCH$_3$)$_2$-4-Cl-Phenyl	4.11 μM	4.12 μM

Ar	MDA-MB-468	MCF-7
5 4-OCH$_3$-Phenyl	1.80 μM	2.90 μM
6 3,5-Cl$_2$-Phenyl	6.90 μM	9.70 μM
7 3,5-(OCH$_3$)$_2$-4-Cl-Phenyl	6.30 μM	7.40 μM

8

MCF-7 6.81 μM

Topoisomerase II 2.52 μM

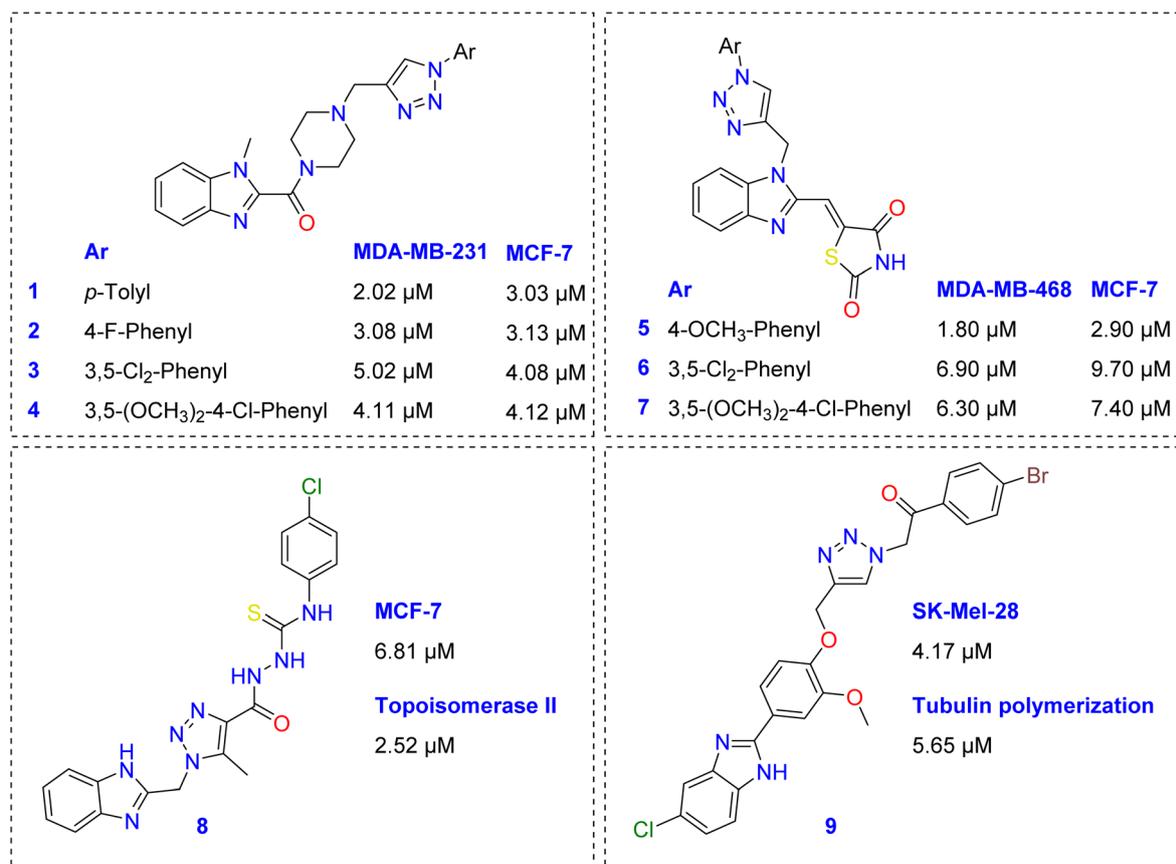**9**

SK-Mel-28 4.17 μM

Tubulin polymerization 5.65 μM

Fig. 1 Representative benzimidazole-1,2,3-triazole hybrids as effective cytotoxic agents and inhibitors of topoisomerases and tubulin polymerization.
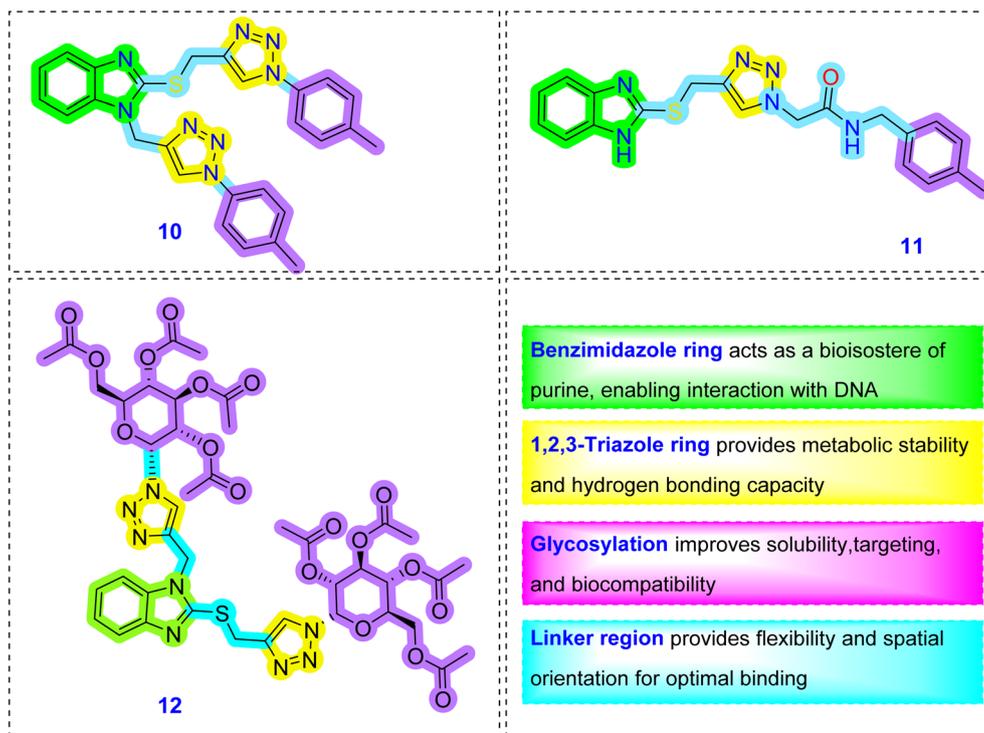
Fig. 2 Pharmacophore features of the designed cytotoxic molecules (**10–12**). Compound **12** incorporates a D-glycosylated benzimidazole-1,2,3-triazole hybrid scaffold bearing acetyl-protected hydroxyl groups and a thioether linker, designed to enhance aqueous solubility and facilitate GLUT-mediated uptake in cancer.

topoisomerase II inhibition and selective cytotoxicity toward MCF-7 cells.[59,63] These findings highlight the dual mechanism of such hybrids involving microtubule disruption and DNA intercalation. Complementarily, Singh *et al.*[56] and Blagojevic and Kamaly[34] reviewed recent advances in nanogel-based delivery of heterocyclic drugs, emphasizing improved solubility, stability, and targeted release profiles. Collectively, these studies provide the conceptual and methodological foundation for the present work, which integrates pharmacologically active benzimidazole–triazole hybrids within chitosan/PVP nanogels to achieve enhanced selectivity and therapeutic performance against mucosal and epithelial cancers.

Compounds **1–9** are cited from previously published studies as representative benzimidazole-1,2,3-triazole hybrids with established anticancer activity, included here solely to illustrate the structural and biological foundation for our current design strategy. In contrast, compounds **10–12** represent the newly designed and synthesized derivatives that constitute the core focus of this study. Structurally, the earlier compounds (**1–9**) comprise benzimidazole-1,2,3-triazole hybrids with varied aromatic or heteroaromatic substituents influencing cytotoxic potency, whereas the new series (**10–12**) incorporate glycosylated, thioether-linked, and acetyl-protected functional groups designed to improve aqueous solubility, lipophilic balance, and receptor-mediated tumor targeting. These features mark a distinct physicochemical and functional advancement, enhancing nanogel encapsulation efficiency and selectivity toward breast and colorectal cancer cells.

The benzimidazole-1,2,3-triazole hybrids combine two pharmacologically active heterocycles known for their anticancer potential, including inhibition of tubulin polymerization and topoisomerase activity.[38,40,48,49,58] As well, the integration of 1,2,3-triazole-benzimidazole hybrids with sugar moieties within nanogel systems represents a promising strategy for enhancing targeted drug delivery in breast cancer therapy.[17] This last approach combines the pharmacological potency of heterocyclic scaffolds with the biological targeting capabilities of carbohydrate units. Sugar moieties can bind to overexpressed glucose transporters (GLUTs) or lectin receptors on breast cancer cells, facilitating selective uptake and improving intracellular drug delivery.[64] Additionally, glycosylation improves the aqueous solubility and stabilizes the nanogel matrix, allowing for controlled and sustained release of therapeutics.[65,66] Anticancer candidates incorporating benzimidazole and 1,2,3-triazole cores are expected to contribute to apoptosis induction,[67] cell cycle arrest, and enzyme inhibition (*e.g.*, tubulin and topoisomerase), while sugar conjugation enhances selectivity, bioavailability, and the drug delivery to aggressive cancers like Triple-Negative Breast Cancer (TNBC). Based on the aforementioned scientific facts and in continuation of our research efforts to develop effective bioactive candidates,[68–71] we designed a nanogel formulation to deliver three chemical entities into breast cancer cells. In our designed molecules **10–12** (Fig. 2), the incorporation of benzimidazole and 1,2,3-triazole rings, well-known anticancer pharmacophores, has been considered. These rings are often used in medicinal chemistry

for topoisomerase inhibition and DNA intercalation.[38,48,49,58] The benzimidazole ring acts as a bioisostere of purine,[5] enabling interaction with DNA and enzymes. 1,2,3-Triazole provides metabolic stability and hydrogen bonding capacity, enhancing binding affinity to biological targets. One of the designed molecules shows a multiple acetylated sugar unit (a glycosylated 1,2,3-triazole-benzimidazole hybrid conjugate). This glycosylation is expected to improve water solubility and to allow for receptor-mediated targeting for the high glucose demand cells Caco-2 and MDA-MB-231.[72,73] It also enhances the selectivity of tumor cells over normal cells. Acetylation of the sugar moiety was designed to protect hydroxyl groups and to modulate lipophilicity. This action makes the molecule act as a prodrug, releasing active compounds upon enzymatic cleavage in the tumor environment. Finally, the linker region (thioether and methylene bridge) provides flexibility and spatial orientation required for optimal binding and proper alignment of pharmacophores within the target binding site.

2 Results and discussion

2.1 Molecular design rationale

The structural design of compounds 10–12 was guided by integrating two bioactive heterocycles: benzimidazole and 1,2,3-triazole, known for their anticancer and enzyme–inhibitory profiles. The benzimidazole moiety was selected to facilitate DNA intercalation and topoisomerase inhibition, while the 1,2,3-triazole linker ensured molecular rigidity and additional hydrogen-bonding capacity. The attachment of glycosyl and acetyl-protected units was intended to enhance hydrophilicity and promote selective internalization via glucose transporter mechanisms in cancer cells. The incorporation of thioether linkers improved conformational flexibility, supporting optimal interaction with target binding sites. Together, these rational modifications balanced hydrophilic–lipophilic properties, improved nanogel encapsulation, and contributed to the observed enhancement in biological activity and selectivity of the nanogel formulations.

2.2 UV-vis spectrophotometric analysis

Fig. 3 displays the UV-Vis absorption spectra of three drug candidates (10, 11, and 12) in their free form (curve 1) and after encapsulation within the CPPNs system (10ng, 11ng, and 12ng)

(curve 2). The UV-Vis spectra provide critical insights into the molecular interactions between the drug molecules and the nanogel matrix, as well as the changes in their optical properties upon encapsulation. The UV-Vis spectra highlighted distinct structure-dependent behaviors of the free drugs and their nanogel-encapsulated counterparts. 10ng, with extended aromatic conjugation and electron-donating substituents, exhibited strong absorption and a slight bathochromic shift after encapsulation. This indicates π–π interactions and stabilization of the drug within the CPPNs network. In contrast, 11ng, which contains fewer conjugated groups and more polar substituents, showed weaker absorption and a hypsochromic shift, suggesting restricted electron delocalization within the polymeric environment. 12ng, characterized by bulky hydrophobic substituents, displayed broad absorption bands in its free form, which became sharper upon encapsulation. This reflects improved solubilization and reduced aggregation due to confinement within the nanogel matrix. Finally, Fig. 3 confirms the successful encapsulation of drug candidates within the CPPNs system, demonstrating its potential for drug delivery applications by modulating drug solubility, stability, and controlled release properties.

2.3 Dynamic light scattering (DLS) analysis

Fig. 4 presents the hydrodynamic diameter distributions of the three drug-loaded CPPNs (10ng, 11ng, and 12ng) measured using dynamic light scattering (DLS). DLS is a widely used technique for determining the size and dispersity of nanoparticles by analyzing their Brownian motion in suspension. The hydrodynamic diameter obtained from DLS accounts for the nanoparticle core along with its associated solvation layer, making it an essential parameter for evaluating colloidal stability. The intensity-weighted size distribution profiles of all three drug-loaded nanogels exhibit monomodal peaks, indicating a relatively uniform nanoparticle population with minimal aggregation. Additionally, the polydispersity index (PDI) values remain below 0.3, suggesting high formulation stability and narrow size distribution. Such characteristics are advantageous for biomedical applications, as they contribute to consistent drug release kinetics and improved biological performance.

DLS analysis further confirmed that the hydrodynamic size and stability of the nanogels were strongly influenced by
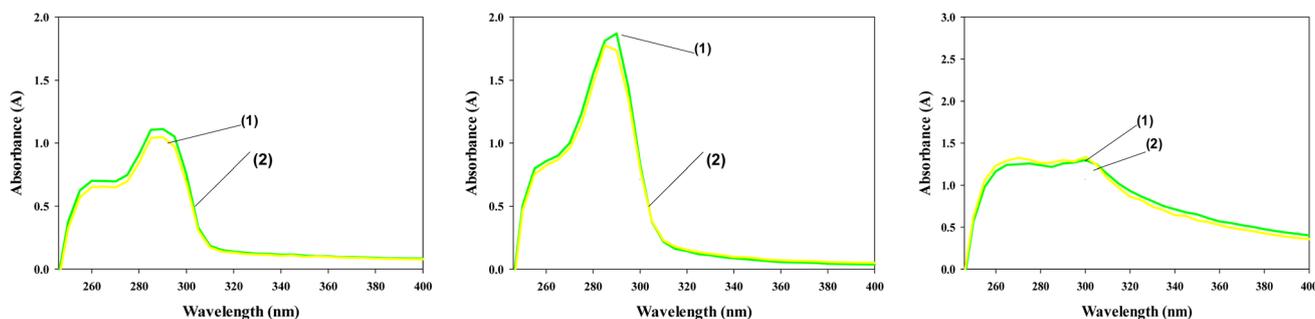

Fig. 3 UV spectrophotometer of 10ng (left), 11ng (middle), and 12ng (right) presented as free samples curve 1 and nanogel curve 2.

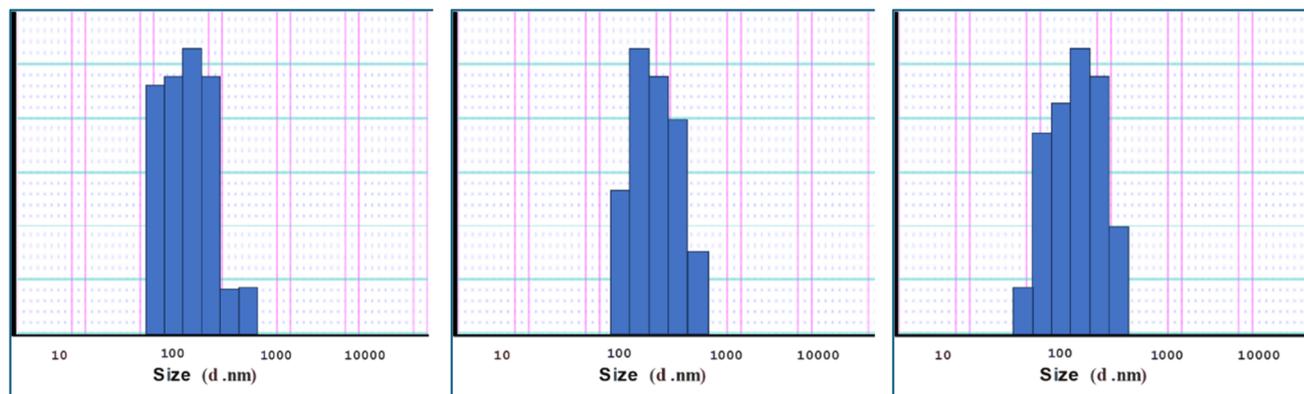**Fig. 4** Dynamic light scattering analyses of **10ng** (left), **11ng** (middle), and **12ng** (right).

molecular structure. **10ng** nanogels displayed the smallest size (~100–150 nm) with a narrow polydispersity index (PDI), consistent with efficient encapsulation and strong drug–polymer compatibility. **11ng** nanogels were moderately larger (~180–200 nm) and exhibited a broader PDI, reflecting weaker interactions with the CPPNs network. **12ng** nanogels showed the largest sizes (~220–250 nm) and the broadest PDI, which can be attributed to steric hindrance from hydrophobic substituents and, accordingly, lower tendency for aggregation.

Variations in particle size among the three different formulations may be attributed to differences in drug–polymer interactions, encapsulation efficiency, and the degree of cross-linking within the nanogel matrix. Despite these variations, all three formulations maintain their nanoscale dimensions, confirming the suitability of the CPPNs for controlled drug delivery. Their controlled size and stability reinforce their potential for biomedical applications, particularly in improving drug solubility, bioavailability, and sustained release. These findings confirm that extended conjugation and balanced polarity in **10ng** promote tighter nanogel packing and superior colloidal stability.

2.4 Stability evaluation of nanogels

The dynamic light scattering (DLS) analysis, shown in Fig. 4, demonstrates that the **12ng** exhibits excellent structural integrity during the initial phase of stability testing under physiologically relevant conditions. By day 2, the DLS profile revealed a sharp, monomodal distribution centered around approximately 183 nm, closely mirroring the characteristics of the blank sample in Fig. 4 and indicating preserved colloidal stability, with no significant aggregation or degradation, within the first 48 hours of incubation in PBS at 37 °C and simulated body fluids. By Day 5, a slight but discernible shift to the right in the hydrodynamic diameter was observed, accompanied by a modest broadening of the size distribution. This change suggests the onset of minor particle swelling or early-stage aggregation, likely resulting from gradual relaxation of the polymer network or electrostatic screening of chitosan's cationic groups in the high-ionic-strength medium. Despite these changes, the nanogels maintained a predominantly

monodisperse profile, confirming their continued stability at this intermediate time point. On Day 7, a more pronounced increase in particle size was evident, with the distribution centering near 200 nm and exhibiting broader polydispersity. This progression reflects enhanced intermolecular interactions among nanogel particles, potentially driven by partial polymer degradation or ion-mediated cross-linking. Although the system remained within the nanoscale range, the increased heterogeneity signaled a noticeable decline in colloidal stability compared to earlier intervals. By Day 10, a marked shift in the DLS profile was apparent, with the hydrodynamic diameter extending toward 205–212 nm and significant tailing in the distribution, indicative of aggregate formation. This evolution underscores long-term stability under physiological stress (Fig. 5).

2.5 Transmission electron microscope (TEM) analysis

Fig. 6 displays high-resolution TEM images of the three drug-loaded CPPNs (**10ng**, **11ng**, and **12ng**), providing critical insights into their morphology, size distribution, and structural integrity.[74] The TEM micrographs reveal spherical nanoparticles with smooth surfaces and uniform shapes across all formulations, confirming the successful synthesis of well-defined nanogels. The observed particle sizes in the dry state, as imaged by TEM, range between 80–150 nm, which is slightly smaller than the hydrodynamic diameters measured by DLS (Fig. 4). The TEM images demonstrate homogeneous dispersion of the nanogels, with no visible aggregates or irregular structures, aligning with the low polydispersity indices (PDI < 0.3) observed in the DLS data.

TEM imaging provided morphological confirmation of the DLS data. All nanogels displayed spherical morphology. However, the degree of uniformity varied with drug structure. **10ng** nanogels were highly monodisperse with smooth, well-defined boundaries, confirming efficient structural embedding within the PPAN framework. **11ng** nanogels were less uniform, while **12ng** nanogels exhibited clustering and aggregation, consistent with steric constraints imposed by bulky hydrophobic substituents. As expected, TEM sizes were slightly smaller than DLS values due to the absence of hydration shells.
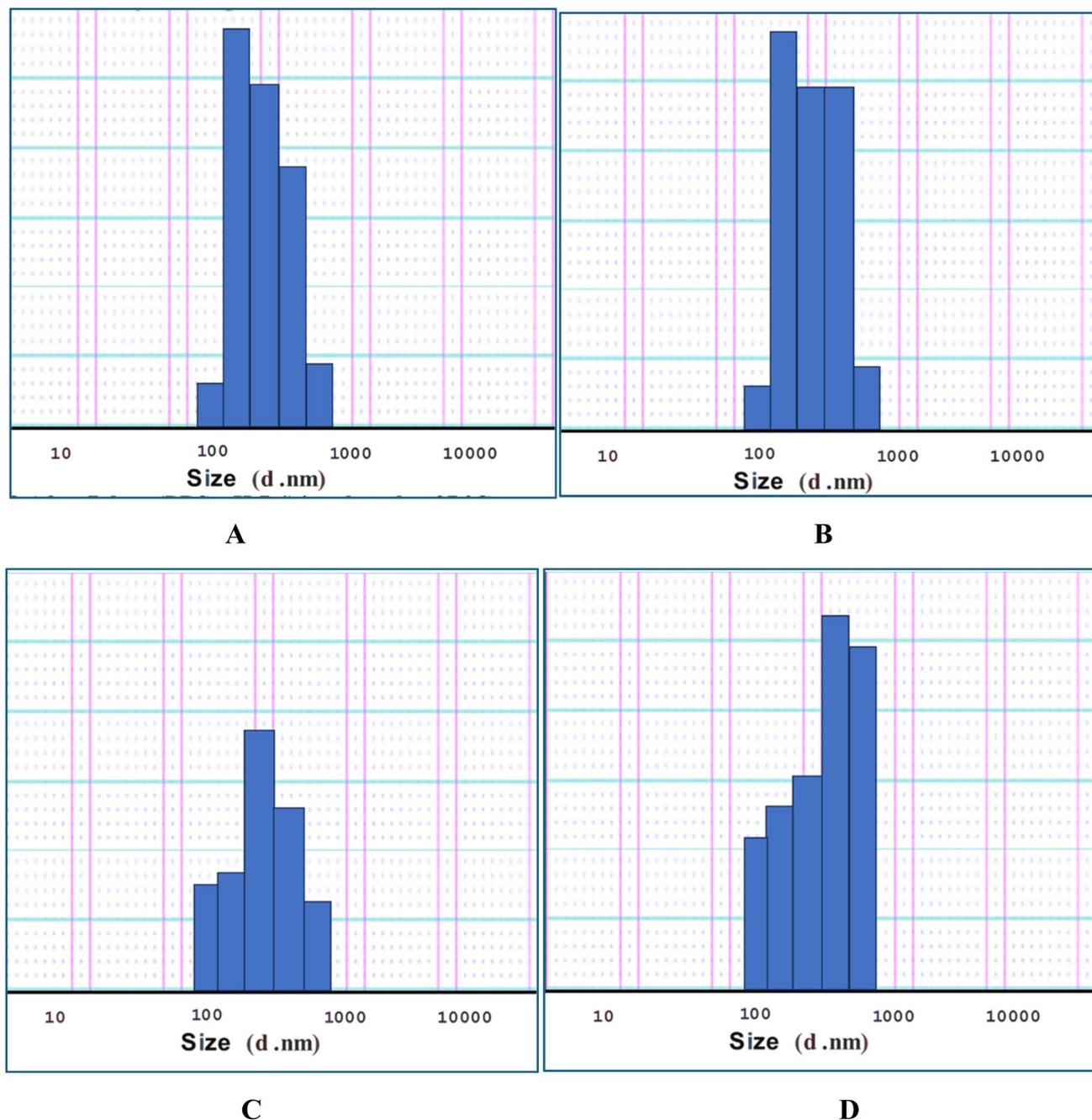
Fig. 5 DLS stability evaluation of **12ng** nanogel in PBS at PH 7.4 for distinct days. (A) After 2 days; (B) after 5 days; (C) after 7 days; (D) after 10 days.

The spherical morphology is consistent with the self-assembly behavior of CPPNs, where cross-linking during synthesis promotes the formation of compact, globular structures. Additionally, the absence of phase separation or distinct drug crystals within the nanogel matrix, evidenced by the lack of dark spots or irregular contrasts, supports the UV-Vis findings (Fig. 3), which suggested physical entrapment rather than chemical bonding or surface adsorption of the drugs. Further examination of specific samples reveals subtle structural variations. Sample **10ng** exhibits a slightly denser core, suggesting localized drug accumulation within the nanogel matrix. **11ng**

presents a marginally larger particle size ($\sim$140 nm), correlating well with the DLS-derived hydrodynamic diameter ($\sim$160 nm), indicating mild swelling due to drug loading. Sample **12ng** displays uniform contrast across the nanoparticles, implying even drug distribution within the polymeric network, with no evidence of surface defects. These observations highlight the influence of drug encapsulation on nanogel structure.

2.6 Comparative structure–property correlation

The physicochemical characteristics of **10ng**, **11ng**, and **12ng** were significantly affected by nanogel formulations (Table 2).
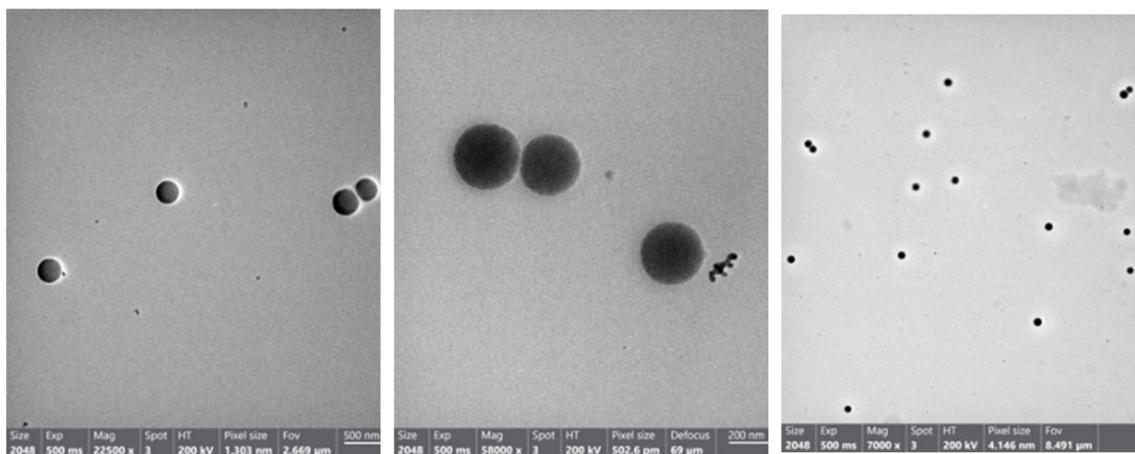
Fig. 6 High-resolution transmission electron microscope images of CPPNs loaded with **10ng** (left), **11ng** (middle), and **12ng** (right).

Table 2 Correlation between the chemical structures of **10ng**, **11ng**, and **12ng** and their physicochemical characteristics

Cpd.	Structural features	UV-vis behavior	DLS results	TEM morphology
10ng	Extended conjugation; balanced hydrophilic–lipophilic profile	Strong absorption; slight bathochromic shift due to π–π interactions with CPPNs	Smallest size ($\sim$100–150 nm), narrow PDI; high stability	Monodisperse, spherical, smooth surface; highly uniform
11ng	Reduced conjugation; more polar substituents	Weaker absorption; hypsochromic shift reflecting restricted delocalization	Moderate size ($\sim$180–200 nm); broader PDI than **10ng**	Spherical, less uniform; moderate stability
12ng	Bulky hydrophobic substituents; steric hindrance	Broad peaks in free form; sharper after encapsulation, indicating improved solubilization	Largest size ($\sim$220–250 nm), broadest PDI; tendency to aggregate	Spherical with clusters irregular distribution

Collectively, all these previous findings highlight the crucial role of structural features in governing the physicochemical performance of nanogel formulations. **10ng**, with its extended conjugation and balanced substituents, demonstrated superior encapsulation, stability, and morphology, making it the most promising candidate for further biological evaluation. **11ng** showed moderate performance, while **12ng** suffered from aggregation and size heterogeneity due to bulky hydrophobic substituents. These results underscore the importance of rational structural design in optimizing nanogel-based drug delivery systems.

2.7 Cytotoxicity assay

Cytotoxic activity of the target compounds in their nanogel formulations (**10ng**, **11ng**, and **12ng**) was evaluated on two mucosal and epithelial cancer cells (MDA-MB-231 and Caco-2). Compared to their free forms (**10**, **11**, and **12**), all compounds in nanogel formulation enhanced the cytotoxic activity in both cancer cells. In the case of **12ng**, the cytotoxicity performance surpasses that of the reference drug staurosporin. This enhancement is evident against both cancer cell lines, where **12ng** exhibited IC$_{50}$ values of 3.13 µM and 3.64 µM, against MDA-MB-231 and Caco-2, respectively, while staurosporin

displayed IC$_{50}$ values of 3.57 µM and 4.60 µM. These values represent substantial potency gain compared to the free form of compound **12** (16.48 µM and 7.90 µM, respectively). This result suggested that nanogel encapsulation enhances cellular uptake, increases aqueous solubility, and possibly prolongs intracellular retention. In parallel, the other couple of compounds obey the same activity pattern. The nanogel formulation **10ng** showed IC$_{50}$ values of 5.41 µM and 12.20 µM, against MDA-MB-231 and Caco-2, respectively, while its free form displayed IC$_{50}$ values of 31.44 µM and 43.94 µM. The nanogel formulation **11ng** showed IC$_{50}$ values of 4.10 µM and 8.29 µM, against MDA-MB-231 and Caco-2, respectively, compared to the free form, which displayed IC$_{50}$ values of 68.35 µM and 63.81 µM. This means that the relative potency of **11ng** on MDA-MB-231 and Caco-2 cells is 16.64-fold and 7.69-fold, respectively, compared to its' free form, Table 3, Fig. 7.

Cytotoxic activity of the target compounds was also investigated against a non-cancerous cell (HEK-293) to evaluate their safety and selectivity profiles. Nanogel formulation also improved the selectivity indices (SI) of the studied compounds. Regarding MDA-MB-231 cells, the SI of **12ng** was found to be 11.74, which is more than fifteen times the SI of the free form (Table 4). In Caco-2, **12ng** showed more than a two-fold SI compared to its free form.

Table 3 Cytotoxic activity of the target compounds against different cell lines

Cpd.	IC$_{50}$ (µM)^a			SI^b	
	MDA-MB-231	Caco-2	HEK-293	HEK/MDA	HEK/Caco-2
10	31.44 ± 2.02	43.94 ± 1.521	77.58 ± 3.55	2.47	1.40
11	68.35 ± 3.099	63.81 ± 1.09	63.41 ± 2.50	0.93	0.93
12	16.48 ± 2.01	7.90 ± 1.51	12.48 ± 1.04	0.76	0.48
10ng	5.41 ± 0.81	12.20 ± 1.67	30.20 ± 1.67	5.58	2.25
11ng	4.10 ± 0.54	8.29 ± 0.51	17.67 ± 1.50	4.30	2.02
12ng	3.13 ± 0.22	3.64 ± 0.25	36.86 ± 2.62	11.74	1.16
CPPNs	>100	>100	>100	NA	NA
Staur.^{c}	3.57 ± 0.07	4.60 ± 0.21	11.85 ± 0.75	3.32	1.29

^{a} IC$_{50}$ values shown here are expressed as the mean values of three experiments and are reported as the mean $\pm$ standard error. All data are reported for free drugs, nanogels, and free nanogel. ^{b} SI = selectivity index. ^{c} Staur. = staurosporin.

2.8 Enzyme assay on topoisomerases I and II and tubulin polymerization

Both the free and nanogel forms of the benzimidazole-based anticancer candidates were tested for their potential to inhibit topoisomerase I (Topo I), topoisomerase II (Topo II), and tubulin polymerase. Each candidate was tested in both its free and nanogel-encapsulated forms against two cancer cell lines: Caco-2 and MDA-MB-231. The detailed percent inhibition

values for all concentrations and formulations are provided in the SI File (Table S2). Three different concentrations (50, 100, and 500 ppm) were tested to evaluate the overall inhibitory potential of the tested anticancer candidates. The geometric meaning of the percent inhibition values was calculated based on the obtained percent inhibition values. The geometric mean was selected as the most appropriate statistical measure due to its ability to reflect nonlinear changes in biological activity,
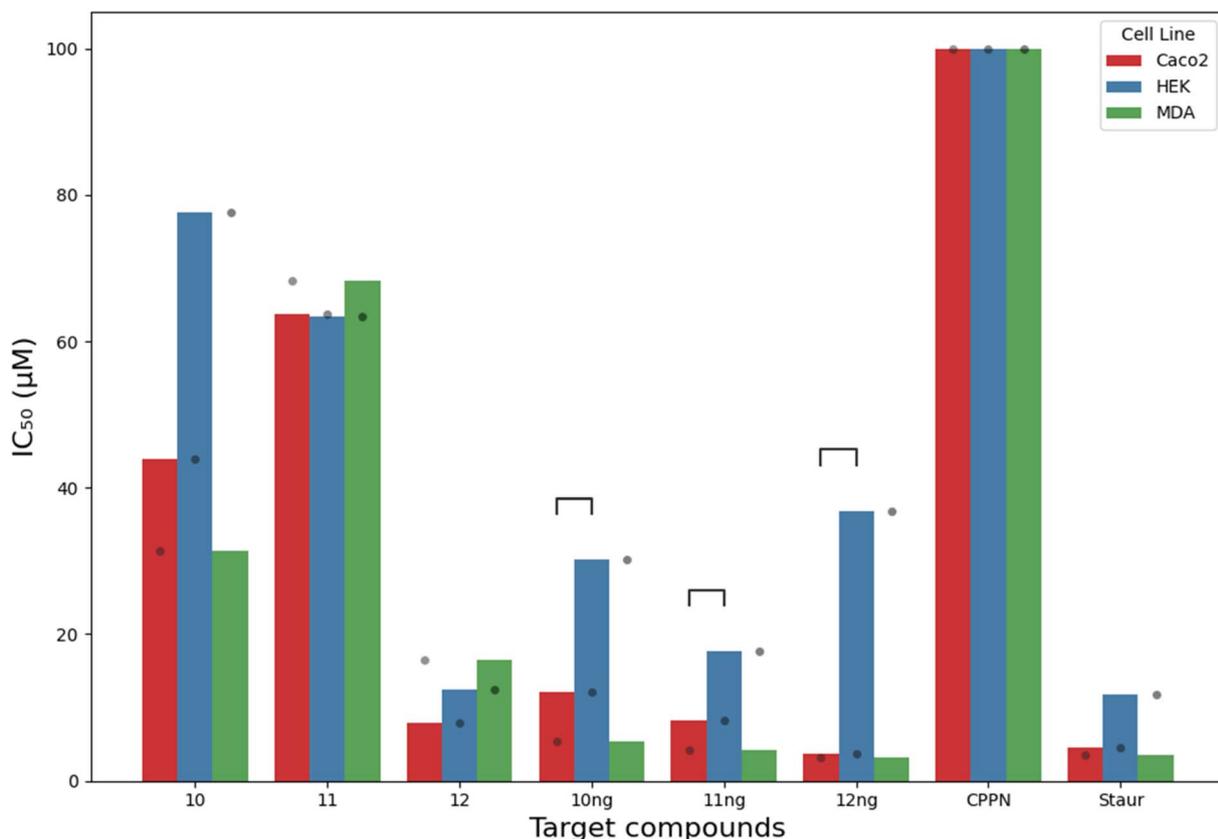

Fig. 7 Cytotoxic activity (IC$_{50}$, µM) of compounds **10–12**, their nanogel formulations (**10ng–12ng**), and reference agents (CPPN and staurosporine) against Caco-2, HEK, and MDA-MB-231 cell lines. Data are presented as mean $\pm$ SE from three independent experiments. The half-bracket symbols indicate statistically significant differences between compared groups, where significance levels are represented as $*p < 0.05$, $**p < 0.01$, and $**p < 0.001$.

Table 4 Comparison of relative potencies and relative selectivity of nanogel formulations *versus* free forms

10ng : 10		11ng : 11		12ng : 12	
Relative potency					
MDA-MB-231	5.81	MDA-MB-231	16.64	MDA-MB-231	5.25
Caco-2	3.60	Caco-2	7.69	Caco-2	2.17
Relative selectivity					
HEK/Caco-2	1.61	HEK/Caco-2	2.16	HEK/Caco-2	2.42
HEK/MDA	2.26	HEK/MDA	4.64	HEK/MDA	15.51

particularly in dose–response relationships. This approach minimizes the influence of extreme values and provides a more representative estimate of the compound's inhibitory efficacy across the tested concentration range.[75–77] As revealed in Fig. 8, the observed percent inhibition values highlight the crucial role of nanogels in potentiating cytotoxic activity through enzyme inhibition. Across all three biological targets, nanogels consistently outperformed the free counterparts. This observation reflects the superior and efficient intracellular uptake of CPPNs compared to free forms. The enhancement was most pronounced for **10ng**, especially against TOPO I in Caco2 (from 28.65% to 63.22%). **12ng** was the most potent overall three biological targets. It achieved 70.45% of the means of inhibition of TOPO I compared to 52.55% of its analogous free counterpart in Caco2. In MDA-MB-231 cells, no significant change has been detected on the effect of Topo I between nanogels and their counterparts. **12ng** also showed strong activity against TOPO II

(63.73% compared to free **12** with 53.09% against MDA-MB-231 cells) and pronounced inhibition of Tubulin (41.82% in MDA-MB-231 cells). While Doxorubicin, the standard drug, remains the most potent for TOPO I and II, **12ng** is comparable for TOPO I in both cancer cells. Paclitaxel remains the most potent Tubulin inhibitor, but **12ng** and **11ng** show partial promising activity in MDA-MB-231.

2.9 Comparative evaluation with previous studies

The cytotoxicity profiles of **10ng–12ng**, particularly **12ng**, compare favorably with previously reported benzimidazole-1,2,3-triazole hybrids and related heterocycles. Earlier studies have described triazolo-linked benzimidazoles with IC_{50} values in the low micromolar range against breast cancer cell lines, mainly acting through tubulin polymerization inhibition, topoisomerase inhibition, and apoptosis induction.[35,40,58,59,62] In the present work, **12ng** exhibited potent cytotoxic activity against MDA-MB-231 and Caco-2 cells (IC_{50} = 3.13 and 3.64 μM, respectively), comparable to or better than several of these previously reported scaffolds, while simultaneously demonstrating improved safety toward normal HEK-293 cells, as reflected by its elevated selectivity indices. Importantly, nanogel encapsulation led to a marked increase in potency and selectivity compared to the corresponding free drugs, with **10ng**, **11ng**, and **12ng** displaying several-fold reductions in IC_{50} values and higher HEK/MDA-MB-231 and HEK/Caco-2 ratios (Tables 3 and 4). These findings are in agreement with earlier reports that chitosan- and PVP-based nanogels can enhance drug solubility, protect labile molecules, and promote tumor-targeted delivery,

Fig. 8 Mean % inhibition activity of compounds 10–12, their nanogel formulations (10ng–12ng), and reference agents on TOPO I, II, and tubulin in Caco2 (upper panel) and MDA–MB-231 (lower panel).

Table 5 Cellular contents (%) of MDA-MB-231 cells after treatment with **12ng** nanogel

Treatment	DNA content %		
	G0/G1	S	G2/M
Control (MDA-MB231)	94.36	4.66	0.98
12ng	96.85	2.89	0.26

resulting in amplified anticancer efficacy and reduced systemic toxicity.[9–12,20,22,26,27,34,56] The superior performance of **12ng** may be attributed to the synergistic integration of benzimidazole and 1,2,3-triazole pharmacophores, the presence of glycosyl and acetyl-protected moieties favoring uptake by glucose-hungry cancer cells, and the CPPN matrix that improves colloidal stability and intracellular accumulation. Altogether, these features distinguish the current nanogel–drug system from previous small-molecule benzimidazole–triazole candidates and conventional nanocarriers by combining potent multitarget activity (Topo I/II and tubulin), enhanced selectivity, and an optimized nanogel-based delivery platform.

2.10 *In vitro* flow cytometric cell cycle analysis

The cell cycle analysis of MDA-MB-231 cells treated with **12ng** nanogel ($IC_{50} = 3.13$ μM) revealed a pronounced arrest in the G0/G1 phase, with 96.85% of cells accumulating in this phase compared to 94.36% in the negative control (Table 5). This effect was accompanied by a reduction in the S and G2/M cellular contents (Fig. 9), suggesting that **12ng** nanogel effectively halts cell cycle progression before DNA synthesis. Cell cycle arrest may be attributed to the molecular interactions of **12ng** with key regulatory proteins involved in cell cycle, such as CDK4 or p21, which are commonly dysregulated in triple-negative breast cancer (TNBC) cells like MDA-MB-231.[78,79]

2.11 Apoptosis induction analysis

The Annexin V/PI staining assay further rationalizes the cytotoxic effect of **12ng** nanogel. Treated cells with a concentration of 3.13 μM; exhibited increased late apoptosis (12.27%) and necrosis (26.85%) compared to control cells (6.56% and 19.30%, respectively), while early apoptosis was reduced from 35.00% to

21.55% (Fig. 10). This pattern suggests that **12ng** nanogel may rapidly drive cells toward irreversible apoptotic and necrotic pathways. The nanogel formulation likely enhances cellular uptake and intracellular retention of **12ng**, facilitating sustained exposure and interaction with apoptotic targets such as caspases or mitochondrial membrane components.

Taken together, these findings indicate that **12ng** nanogel exerts its anticancer effects through a dual mechanism: inducing cell cycle arrest and promoting late-stage apoptosis and necrosis.

2.12 Molecular docking analysis

Driven by its promising results in biological performance, including potent cytotoxicity against MDA-MB-231 ($IC_{50} = 3.13 \pm 0.22$) and Caco-2 ($IC_{50} = 3.64 \pm 0.25$) cancer cell lines, and its superior percent inhibition of Topo I (70.45%), **12ng** has been selected for molecular docking experiment. These experimental findings suggested that **12ng** is a potential candidate for efficient interaction with Topo I, a validated target in cancer therapy. The binding energy of **12ng**, on one hand, was found to be −9.50 kcal mol⁻¹, corresponding to a dissociation constant (K_d) of approximately 110 nM, indicating a moderate binding affinity. On the other hand, the native co-crystallized ligand **FDF** demonstrated a slightly stronger binding profile, with a binding energy of −10.5 kcal mol⁻¹ and a lower K_d of 20 nM. Docking simulations displayed that this candidate engages in multiple stabilizing interactions within the active site of Topo I. It forms hydrogen bonds with residues DT116 (2.43 Å), MET428 (1.94 Å), LYS439 (2.39 Å), and LYS587 (2.09 Å). Additionally, **12ng** participates in π-cation and π–π stacking interactions with DA113 (2.64 Å) and TGP11 (4.09 Å), respectively (Fig. 11). Despite its slightly lower binding affinity, **12ng**'s interaction profile supports its potential as a Topo I inhibitor, especially when considered its strong biological activity and the advantages of nanogel-mediated delivery systems. **FDF** formed hydrogen bonds with ASP533, LYS532, and ARG364 within a distance range of 2.64–3.17 Å, and exhibited extensive π–π stacking interactions with residues such as DA113, TGP11, and DC112. Structural alignment of **12ng** with **FDF** showed a comparable orientation, suggesting that **12ng** may mimic key pharmacophoric features of the native ligand.
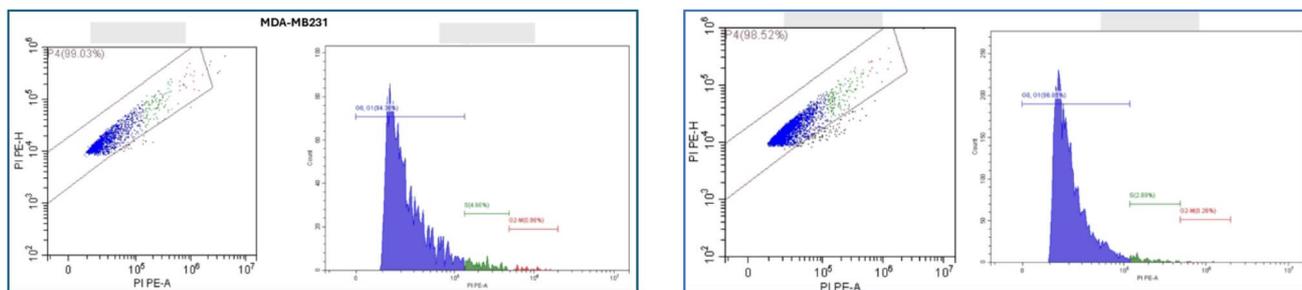

Fig. 9 Histograms of the MDA–MB-231 cells (left) compared with those treated with **12ng** nanogel (right) after incubation with (IC_{50} value) for 24 h. The data is reported as the mean ± SD of three independent experiments in triplicate.
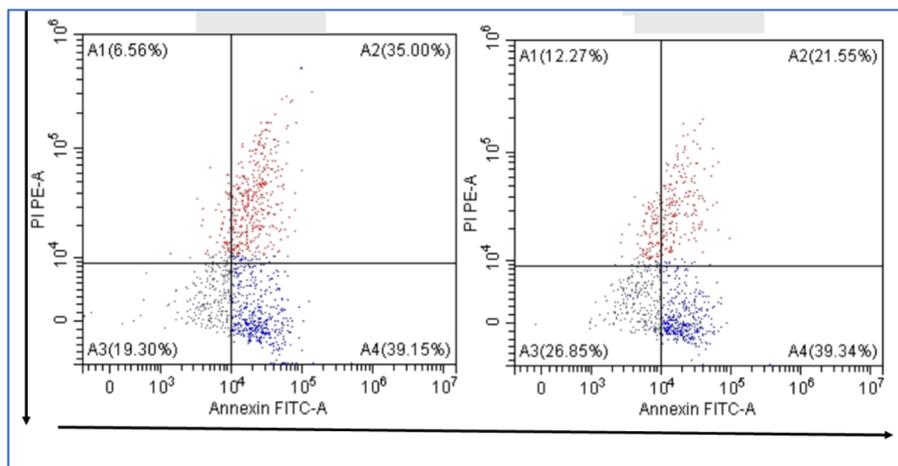
Fig. 10 Annexin V/PI double staining of control MDA-MB-231 (right), and **12ng**-treated cells (left) after incubation with (IC$_{50}$ value) for 24 h. The data is reported as the mean ± SD of three independent experiments in triplicate.
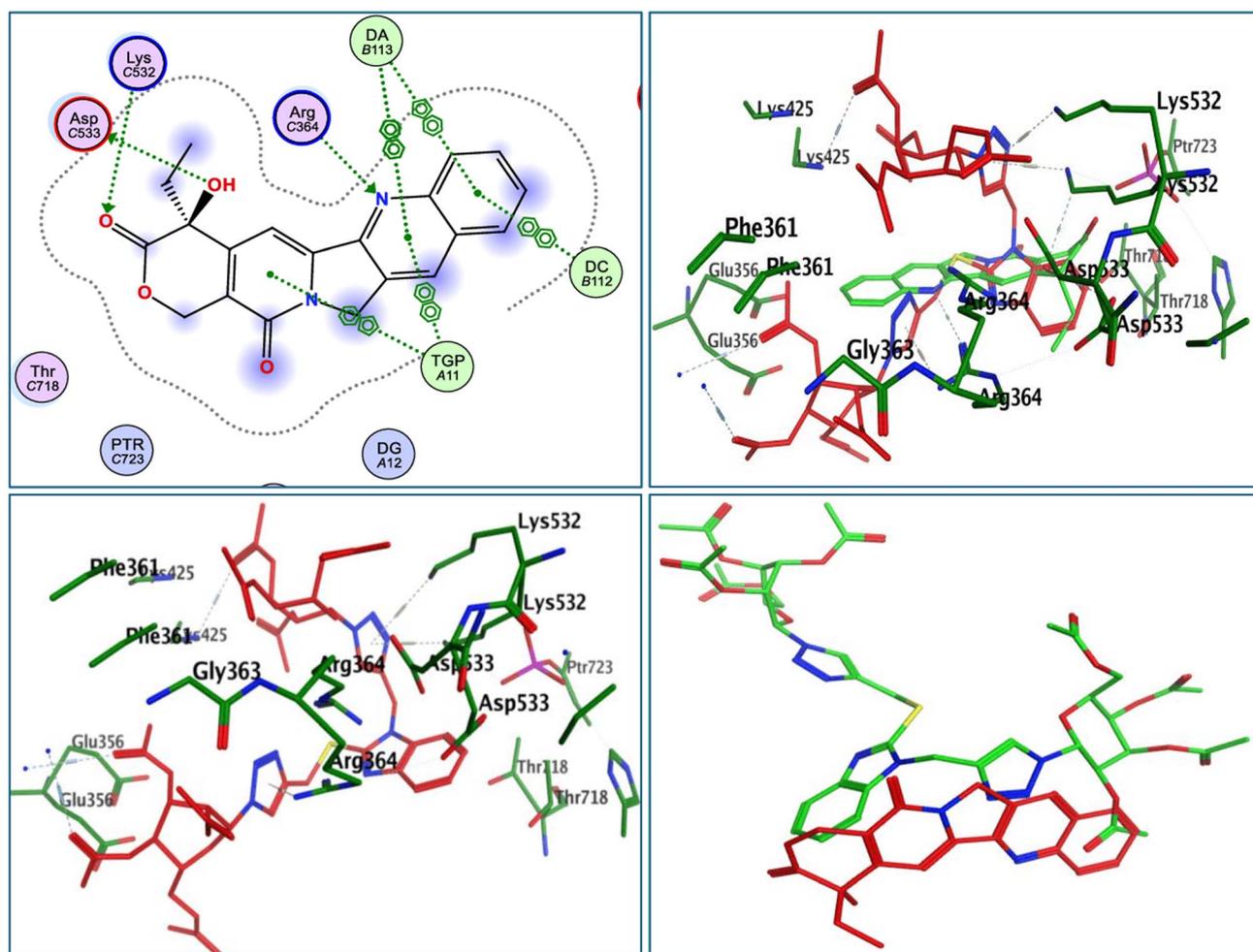

Fig. 11 2D and 3D binding patterns of the native co-crystallized ligand **FDF** (upper panel), binding pattern of **12ng** (lower left), and molecular alignment of both ligands in human DNA topoisomerase I (PDB ID: 1T8I).

3 Conclusion

This study highlights the design and evaluation of multifunctional nanogel systems incorporating benzimidazole-1,2,3-triazole hybrids for targeted treatment of breast and colorectal cancers. CPPNs demonstrated enhanced drug delivery capabilities, improving solubility, cellular uptake, and biological activity of the encapsulated compounds. The nanogel encapsulated form of **12ng** has emerged as the most effective formulation, exhibiting potent cytotoxicity, selective inhibition of topoisomerases and tubulin, and induction of apoptosis. Molecular docking confirmed its favorable interaction with topoisomerase I, supporting its mechanism of action. The integration of pharmacologically active heterocycles with nanogel carriers presents a synergistic approach to overcoming drug resistance and improving therapeutic precision. These results provide a strong foundation for further preclinical development of nanogel-based anticancer therapies. Overall, this work introduces a previously unexplored combination of benzimidazole-1,2,3-triazole hybrids and chitosan/PVP nanogels tailored for mucosal and epithelial cancers. By integrating rational pharmacophore design, glycosylation-based targeting, and a CPPN carrier, together with a comprehensive mechanistic evaluation, the present study goes beyond conventional "drug-in-nanogel" formulations and provides a distinctive nanoplatform with promising translational potential.

4 Experimental section

4.1 Synthesis and characterization of target compounds

Compounds **10**, **11**, and **12** are structurally distinct benzimidazole-1,2,3-triazole derivatives and are fully described and characterized in the supplementary file and as reported.[35,38,80,81]

4.2 Preparation of chitosan/polyvinyl pyrrolidone (CPPNs)

CPPN nanogels were synthesized by separately dissolving chitosan and PVP in DMSO-based media under controlled stirring and temperature conditions. Chitosan was dissolved at room temperature and adjusted to pH 5.8, while polyvinyl pyrrolidone was heated to 70 °C for complete solubilization. The polymer solutions were blended gradually under vigorous stirring, followed by cross-linking using APS and MBA at 65 °C. The final product was purified *via* dialysis and stored at 4 °C under sterile conditions for further use.[82]

4.3 Drug loading protocol for CPPNs

Three compounds (**10–12**) were individually loaded into CPPNs using a solvent-assisted method. Each sample (150 mg) was dissolved in DMSO and gradually added to the nanogel suspension under controlled stirring. The final concentration was adjusted to 750 ppm. After homogenization and vacuum treatment, formulations were stored at 4 °C in light-protected conditions. All preparations were performed aseptically and characterized within 24 hours to ensure uniformity and stability.[83]

4.4 Characterization of nanogels

The physicochemical and structural properties of the synthesized drug-loaded CPPNs were comprehensively evaluated using a complementary suite of analytical techniques. UV-Visible spectrophotometric analysis was conducted on an Agilent Cary 60 spectrophotometer equipped with a xenon flash lamp and dual silicon diode detectors. Particle size distribution, polydispersity, and surface charge characteristics were meticulously determined using a Malvern Zetasizer Nano ZS90 equipped with a 4 mW He–Ne laser ($\lambda = 633$ nm) and an avalanche photodiode detector at a fixed backscattering angle of 173°. Dynamic light scattering measurements were performed in triplicate at 25 °C after a 120 seconds equilibration period, with each measurement consisting of 12 runs of 15 seconds duration. Samples were prepared by diluting the nanogel suspensions (1 : 40) in filtered (0.22 μm) ultrapure water, adjusted to pH 5.5, to achieve an optimal attenuator setting of 6–8 and a count rate of 200–300 kcps. A stability study of CPPNs was conducted using freshly prepared (chitosan/PVP)/TRZS nanogel suspensions, which were subjected to accelerated stability studies under physiologically relevant conditions. Aliquots (2 mL) were diluted 1 : 40 with sterile phosphate-buffered saline (PBS, pH 7.4) and simulated body fluid (SBF, pH 7.4), transferred into sterile Eppendorf tubes, and incubated at 37 °C in a controlled CO_2 incubator. These conditions were selected to mimic the physiological environment and evaluate the colloidal stability of the nanogels. Samples were withdrawn at predetermined intervals of 2, 5, 7, and 10 days for subsequent analysis. Samples were prepared by diluting the nanogel suspensions (1 : 40) in filtered (0.22 μm) ultrapure water adjusted Aliquots (2 mL) were diluted 1 : 40 with sterile phosphate-buffered saline (PBS, pH 7.4) and simulated body fluid (SBF, pH 7.4), transferred into sterile Eppendorf tubes, and incubated at 37 °C to mimic *in vivo* conditions. The stability of the nanogels was evaluated over predetermined intervals of 2, 5, 7, and 10 days.

High-resolution morphological characterization was performed using a JEOL JEM-2100F transmission electron microscope operating at an accelerating voltage of 200 kV with a point resolution of 0.19 nm. Nanogel suspensions were diluted to 0.01% w/v and deposited onto carbon-coated copper grids (400 mesh).

4.5 Cytotoxicity evaluation using a viability assay

The cytotoxic activity was assessed using the 3-(4,5-dimethylthiazol-2-yl)-2,5-diphenyl tetrazolium bromide (MTT) colorimetric assay as reported previously.[84,85]

4.6 Topoisomerase I/II enzyme assay

The inhibitory activity against topoisomerase I was assessed using purified enzyme derived from calf thymus, whereas human-derived topoisomerase II was employed for its corresponding assay. Experimental procedures were conducted using commercial assay kits obtained from TopoGen Inc. (Port Orange, FL), following the manufacturer's recommended

protocol. All mixtures were incubated at 37 °C for 30 minutes in the presence of dimethyl sulfoxide (DMSO) as the solvent. Post-incubation samples were subjected to agarose gel electrophoresis without ethidium bromide. Subsequently, gels were stained with ethidium bromide, rinsed, and imaged to visualize DNA relaxation and cleavage patterns.

4.7 Cell cycle analysis

Cell cycle distribution analysis was assessed using the Propidium Iodide Flow Cytometry followed by flow cytometry analysis.[2] The DNA contents were determined by a FACS Caliber flow cytometer. Finally, cell cycle phase distribution was analyzed using Cell Quest Pro software.

4.8 Quantification of apoptosis

Annexin V-FITC apoptosis assay was performed by using Annexin V-FITC/PI double staining detection kit.[5,86] Flow cytometry analysis was performed using a FACS Caliber flow cytometer (BD Biosciences, Franklin Lakes, NJ, USA). Annexin V-FITC was detected through the (FL1) channel, while PI was detected through the (FL2) channel. Finally, a minimum of 10 000 cells per sample were acquired and analyzed using Cell Quest Pro software (BD Biosciences).

4.9 In vitro tubulin polymerization assay

The *in vitro* tubulin polymerization assay was performed utilizing the nanogels: **10ng**, **11ng**, and **12ng**, compared to free compounds **10**, **11**, and **12**, using the MD-MBA-231 cell line according to the manufacturer's instructions (Cytoskeleton, Cat# BK006P).

4.10 Docking experiments

Molecular docking studies were carried out using AutoDock Tools,[87] while docking simulations were conducted with PyRx.[88] Visualization and analysis of docking interactions were carried out using Discovery Studio Visualizer. The three-dimensional crystallographic structure of human DNA topoisomerase I (PDB ID: 1T8I; https://www.rcsb.org/structure/1T8I) was retrieved from the Protein Data Bank and used as the macromolecular target. The protein was prepared using AutoDock Tools by adding hydrogen atoms consistent with a physiological pH of 7.0 and removing all water molecules. The binding site was defined based on the coordinates of the co-crystallized ligand allowing for a comprehensive exploration of the active pocket. Ligand structure for compound **12** was generated and energy-minimized. Docking simulations were performed using the Lamarckian Genetic Algorithm (LGA) in AutoDock, and the most favorable binding conformations were selected based on binding free energy scores. Post-docking visualization and interaction analysis were conducted in PyMOL (version 2.4) to examine hydrogen bonding, hydrophobic contacts, and π–π stacking interactions. The predicted poses were compared to the co-crystallized ligand to evaluate docking accuracy and deduce inhibitory potential. Root Mean Square Deviation (RMSD) values were calculated by superimposing the docked ligands on the co-crystallized reference structure. For further structural refinement, quantum mechanical calculations and surface molecular orbital analyses were performed using the Gaussian 9.0 software, employing the B3LYP functional for geometry optimization.[89]

Conflicts of interest

The authors declare that he has no conflict of interest.

Data availability

Data used for the research described in the article and supplementary information (SI) file. Supplementary information is available. See DOI: https://doi.org/10.1039/d5ra07972a.

Acknowledgements

References

1 *Breast cancer*, https://www.who.int/news-room/fact-sheets/detail/breast-cancer, accessed September 30, 2025.

2 E. M. Husseiny, H. S. Abulkhair, N. M. El-Dydamony and K. E. Anwer, Exploring the cytotoxic effect and CDK-9 inhibition potential of novel sulfaguanidine-based azopyrazolidine-3,5-diones and 3,5-diaminoazopyrazoles, *Bioorg. Chem.*, 2023, **133**, 106397, DOI: 10.1016/j.bioorg.2023.106397.

3 *Breast cancer cases projected to rise by nearly 40 per cent by 2050*, WHO warns, 2025, https://news.un.org/en/story/2025/02/1160391, accessed September 6, 2025.

4 Y. Xi and P. Xu, Global colorectal cancer burden in 2020 and projections to 2040, *Transl. Oncol.*, 2021, **14**, 101174, DOI: 10.1016/j.tranon.2021.101174.

5 E. M. Husseiny, H. S. Abulkhair, A. Saleh, N. Altwaijry, R. A. Zidan and F. G. Abdulrahman, Molecular overlay-guided design of new CDK2 inhibitor thiazepinopurines: Synthesis, anticancer, and mechanistic investigations, *Bioorg. Chem.*, 2023, **140**, 106789, DOI: 10.1016/j.bioorg.2023.106789.

6 M. Luo, X. Yang, H.-N. Chen, E. C. Nice and C. Huang, Drug resistance in colorectal cancer: An epigenetic overview, *Biochim. Biophys. Acta Rev. Canc*, 2021, **1876**, 188623, DOI: 10.1016/j.bbcan.2021.188623.

7 A. Zafar, S. Khatoon, M. J. Khan, J. Abu and A. Naeem, Advancements and limitations in traditional anti-cancer therapies: a comprehensive review of surgery, chemotherapy, radiation therapy, and hormonal therapy, *Discov. Oncol.*, 2025, **16**, 607, DOI: 10.1007/s12672-025-02198-8.

8 F. G. Abdulrahman, H. S. Abulkhair, H. S. El Saeed, N. M. El-Dydamony and E. M. Husseiny, Design, synthesis, and mechanistic insight of novel imidazolones as potential

EGFR inhibitors and apoptosis inducers, *Bioorg. Chem.*, 2024, **144**, 107105, DOI: 10.1016/j.bioorg.2024.107105.

9 F. ud Din, W. Aman, I. Ullah, O. S. Qureshi, O. Mustapha, S. Shafique and A. Zeb, Effective use of nanocarriers as drug delivery systems for the treatment of selected tumors, *Int. J. Nanomed.*, 2017, **12**, 7291–7309, DOI: 10.2147/IJN.S146315.

10 Z. Edis, J. Wang, M. K. Waqas, M. Ijaz and M. Ijaz, Nanocarriers-Mediated Drug Delivery Systems for Anticancer Agents: An Overview and Perspectives, *Int. J. Nanomed.*, 2021, **16**, 1313–1330, DOI: 10.2147/IJN.S289443.

11 C. Duan, M. Yu, J. Xu, B.-Y. Li, Y. Zhao and R. K. Kankala, Overcoming Cancer Multi-drug Resistance (MDR): Reasons, mechanisms, nanotherapeutic solutions, and challenges, *Biomed. Pharmacother.*, 2023, **162**, 114643, DOI: 10.1016/j.biopha.2023.114643.

12 K. Elumalai, S. Srinivasan and A. Shanmugam, Review of the efficacy of nanoparticle-based drug delivery systems for cancer treatment, *Biomed. Technol.*, 2024, **5**, 109–122, DOI: 10.1016/j.bmt.2023.09.001.

13 M. Ali, S. Mir, L. I. Atanase, O.-U.-R. Abid and M. Kazi, Chitosan–PVA–PVP/nano-clay composite: a promising tool for controlled drug delivery, *RSC Adv.*, 2024, **14**, 15777–15790, DOI: 10.1039/D4RA02959C.

14 C. N. Minh Hoang, S. H. Nguyen and M. T. Tran, Nanoparticles in cancer therapy: Strategies to penetrate and modulate the tumor microenvironment – A review, *Smart Mater. Med.*, 2025, **6**, 270–284, DOI: 10.1016/j.smaim.2025.07.004.

15 M. A. Samad, I. Ahmad, T. A. Zughaibi, M. Suhail, S. K. Zaidi, F. A. Al-Abbasi and S. Tabrez, Nanotechnology-based drug delivery for breast cancer treatment: Current applications and future directions, *Eur. J. Med. Chem. Rep.*, 2025, **14**, 100268, DOI: 10.1016/j.ejmcr.2025.100268.

16 V. C. Deivayanai, P. Thamarai, S. Karishma, A. Saravanan, P. R. Yaashikaa, A. S. Vickram, R. V. Hemavathy, R. R. Kumar, S. Rishikesavan and S. Shruthi, Advances in nanoparticle-mediated cancer therapeutics: Current research and future perspectives, *Cancer Pathog. Ther.*, 2025, **3**, 293–308, DOI: 10.1016/j.cpt.2024.11.002.

17 B. G. Davis and M. A. Robinson, Drug delivery systems based on sugar-macromolecule conjugates, *Curr. Opin. Drug Discov. Devel.*, 2002, **5**, 279–288. http://www.ncbi.nlm.nih.gov/pubmed/11926134.

18 H. S. Abulkhair, α-Glucosidase-targeting 1,2,4-triazole antidiabetic candidates: Comparative analysis and future perspectives, *Future Med. Chem.*, 2025, **18**, 1–16, DOI: 10.1080/17568919.2025.2587561.

19 L.-M. Rečnik, W. Kandioller and T. L. Mindt, 1,4-Disubstituted 1,2,3-Triazoles as Amide Bond Surrogates for the Stabilisation of Linear Peptides with Biological Activity, *Molecules*, 2020, **25**, 3576, DOI: 10.3390/molecules25163576.

20 Z. Sun, C. Song, C. Wang, Y. Hu and J. Wu, Hydrogel-Based Controlled Drug Delivery for Cancer Treatment: A Review, *Mol. Pharm.*, 2020, **17**(2), 373–391, DOI: 10.1021/acs.molpharmaceut.9b01020.

21 H. J. Han, C. Ekweremadu and N. Patel, Advanced drug delivery system with nanomaterials for personalised medicine to treat breast cancer, *J. Drug Deliv. Sci. Technol.*, 2019, **52**, 1051–1060, DOI: 10.1016/j.jddst.2019.05.024.

22 Y. Guo, M. Wang, Y. Zhang, Z. Zhao and J. Li, Advanced hydrogel material for colorectal cancer treatment, *Drug Deliv.*, 2025, **32**, 1–33, DOI: 10.1080/10717544.2024.2446552.

23 Z. Feyissa, G. D. Edossa, T. B. Bedasa and L. G. Inki, Fabrication of pH-Responsive Chitosan/Polyvinylpyrrolidone Hydrogels for Controlled Release of Metronidazole and Antibacterial Properties, *Int. J. Polym. Sci.*, 2023, **2023**, 1–18, DOI: 10.1155/2023/1205092.

24 K. Joy, D. Sathya Seeli and M. Prabaharan, Chitosan Nanoparticles: Drug Delivery Carriers in Cancer Therapy, in *Chitosan Biomater. V*, pp. 261–283, 2024, DOI: 10.1007/12_2024_177.

25 A. Aouadi, D. Hamada Saud, A. Rebiai, A. Achouri, S. Benabdesselam, F. Mohamed Abd El-Mordy, P. Pohl, S. F. Ahmad, S. M. Attia, H. S. Abulkhair, A. Ararem and M. Messaoudi, Introducing the antibacterial and photocatalytic degradation potentials of biosynthesized chitosan, chitosan–ZnO, and chitosan–ZnO/PVP nanoparticles, *Sci. Rep.*, 2024, **14**, 14753, DOI: 10.1038/s41598-024-65579-z.

26 M. Ashrafizadeh, K. Hushmandi, S. Mirzaei, S. Bokaie, A. Bigham, P. Makvandi, N. Rabiee, V. K. Thakur, A. P. Kumar, E. Sharifi, R. S. Varma, A. R. Aref, M. Wojnilowicz, A. Zarrabi, H. Karimi-Maleh, N. H. Voelcker, E. Mostafavi and G. Orive, Chitosan-based nanoscale systems for doxorubicin delivery: Exploring biomedical application in cancer therapy, *Bioeng. Transl. Med.*, 2023, **8**, 1–29, DOI: 10.1002/btm2.10325.

27 T. Li, M. Ashrafizadeh, Y. Shang, Y. Nuri Ertas and G. Orive, Chitosan-functionalized bioplatforms and hydrogels in breast cancer: immunotherapy, phototherapy and clinical perspectives, *Drug Discov. Today*, 2024, **29**, 103851, DOI: 10.1016/j.drudis.2023.103851.

28 R. Qaiser, F. Pervaiz, H. Shoukat, H. Yasin, H. Hanan and G. Murtaza, Mucoadhesive chitosan/polyvinylpyrrolidone-co-poly (2-acrylamide-2-methylpropane sulphonic acid) based hydrogels of captopril with adjustable properties as sustained release carrier: Formulation design and toxicological evaluation, *J. Drug Deliv. Sci. Technol.*, 2023, **81**, 104291, DOI: 10.1016/j.jddst.2023.104291.

29 H. Yadav, R. Malviya and N. Kaushik, Chitosan in biomedicine: A comprehensive review of recent developments, *Carbohydr. Polym. Technol. Appl.*, 2024, **8**, 100551, DOI: 10.1016/j.carpta.2024.100551.

30 B. Almohaywi, M. H. Elkomy, M. A. M. Ali, A. K. B. Aljohani, M. S. Abdulrahman, M. M. Elsebaie, A. M. Alhammad, K. A. Aytah, S. M. Alshehri, E. O. Alharbi, R. R. Alharbi and H. E. A. Ahmed, Development of carboximidamide small molecule nanogels as potent antimicrobial functional drug delivery systems, *RSC Adv.*, 2025, **15**, 35941–35960, DOI: 10.1039/D5RA05150A.

31 M. Asim Raza, K. Shahzad, S. Dutt Purohit, S. Hyun Park and S. Soo Han, The fabrication strategies for chitosan/poly(vinyl

pyrrolidone) based hydrogels and their biomedical applications: A focused review, *Polym. Technol. Mater.*, 2023, **62**, 2255–2271, DOI: 10.1080/25740881.2023.2252928.

32 S. A. nohooji, A. Ghadami, M. Pourmadadi, F. Yazdian, A. Kazemi, M. Mirshafiei and S. H. Bastami, Chitosan/Carbon quantum dots/Polyvinylpyrrolidone nanocarrier for enhanced anticancer efficacy of doxorubicin, *Carbohydr. Polym. Technol. Appl.*, 2025, **11**, 100883, DOI: 10.1016/j.carpta.2025.100883.

33 A. Stefanache, I. I. Lungu, N. Anton, D. Damir, C. Gutu, I. Olaru, A. Plesea Condratovici, M. Duceac (Covrig), M. Constantin, G. Calin, L. D. Duceac and M. Boev, Chitosan Nanoparticle-Based Drug Delivery Systems: Advances, Challenges, and Future Perspectives, *Polymers*, 2025, **17**, 1453, DOI: 10.3390/polym17111453.

34 L. Blagojevic and N. Kamaly, Nanogels: A chemically versatile drug delivery platform, *Nano Today*, 2025, **61**, 102645, DOI: 10.1016/j.nantod.2025.102645.

35 M. A. Soliman, H. E. A. Ahmed, E. H. Eltamany, A. T. A. Boraei, A. Aljuhani, S. A. Salama, R. Alghamdi, A. K. B. Aljohani, M. Almaghrabi and M. R. Aouad, Novel bis-benzimidazole-triazole hybrids: anticancer study, in silico approaches, and mechanistic investigation, *Future Med. Chem.*, 2025, **17**, 93–107, DOI: 10.1080/17568919.2024.2437980.

36 E. M. Othman, E. A. Fayed, E. M. Husseiny and H. S. Abulkhair, The effect of novel synthetic semicarbazone- and thiosemicarbazone-linked 1,2,3-triazoles on the apoptotic markers, VEGFR-2, and cell cycle of myeloid leukemia, *Bioorg. Chem.*, 2022, **127**, 105968, DOI: 10.1016/j.bioorg.2022.105968.

37 E. M. Othman, E. A. Fayed, E. M. Husseiny and H. S. Abulkhair, Rationale design, synthesis, cytotoxicity evaluation, and in silico mechanistic studies of novel 1,2,3-triazoles with potential anticancer activity, *New J. Chem.*, 2022, **46**, 12206–12216, DOI: 10.1039/d2nj02061k.

38 M. A. Soliman, E. H. Eltamany, A. T. A. Boraei, M. R. Aouad, A. Aljuhani, B. Almohaywi, A. A. Awaji, R. Alghamdi, A. K. B. Aljohani and H. E. A. Ahmed, Novel Benzimidazole-1,2,3-Triazole Hybrids: Synthesis, Dual Antimicrobial, Anticancer Activity, Mechanistic Insights, and Computational Studies, *ChemistrySelect*, 2025, **10**, 1–21, DOI: 10.1002/slct.202500813.

39 E. M. Husseiny, H. S. Abulkhair, S. S. El-Haddad, N. Osama and M. S. El-Zoghbi, Aminopyridone-linked Benzimidazoles: A Fragment-based Drug Design for the Development of CDK-9 Inhibitors, *Future Med. Chem.*, 2023, **15**, 1213–1232, DOI: 10.4155/fmc-2023-0139.

40 A. Vanaparthy, K. K. Thallapally, D. Banothu, K. Polkampally, R. S. Kondrapolu, S. K. Nukala and R. Manchal, Synthesis and in-vitro anti-EGFR screening of new 1,2,3-triazole-benzimidazole hybrids and insilico studies, *Chem. Biol. Lett.*, 2025, **12**, 1271, DOI: 10.62110/sciencein.cbl.2025.v12.1271.

41 E. M. E. Dokla, N. S. Abutaleb, S. N. Milik, D. Li, K. El-Baz, M.-A. W. Shalaby, R. Al-Karaki, M. Nasr, C. D. Klein, K. A. M. Abouzid and M. N. Seleem, Development of benzimidazole-based derivatives as antimicrobial agents and their synergistic effect with colistin against gram-negative bacteria, *Eur. J. Med. Chem.*, 2020, **186**, 111850, DOI: 10.1016/j.ejmech.2019.111850.

42 S. Abd El-Karim, W. Zaghary, M. Anwar, G. Awad, N. Mahfouz and G. Hussein, Design, Synthesis and Molecular Docking of New Benzimidazole Derivatives of Potential Antimicrobial Activity as DNA Gyrase and Topoisomerase IV Inhibitors, Egypt, *J. Chem.*, 2021, **64**(7), 3817–3839, DOI: 10.21608/ejchem.2021.75953.3714.

43 H. S. Abulkhair, The role of the sulfaguanidine molecular scaffold in drug design and development, *Arch. Pharm.*, 2025, **358**, e2400802, DOI: 10.1002/ardp.202400802.

44 A. Kanwal, M. Ahmad, S. Aslam, S. A. R. Naqvi and M. J. Saif, Recent Advances in Antiviral Benzimidazole Derivatives: A Mini Review, *Pharm. Chem. J.*, 2019, **53**, 179–187, DOI: 10.1007/s11094-019-01976-3.

45 D. G. O'Sullivan and A. K. Wallis, Antiviral benzimidazoles. Direct 1-substitution of 2-(.alpha.-hydroxybenzyl) benzimidazole and related compounds, *J. Med. Chem.*, 1972, **15**, 103–104, DOI: 10.1021/jm00271a032.

46 R. Elrayess, R. Elrayess and N. Abady, Synthesis, Molecular Docking, and Anti-inflammatory Activities of Some Novel Benzimidazole Derivatives as Potential Cyclo-oxygenase-2 Inhibitors, *Egypt. J. Chem.*, 2023, **67**, 255–266, DOI: 10.21608/ejchem.2023.218909.8165.

47 H. S. Abulkhair, Synthetic approaches, biological activity evaluations, and mechanistic investigations of sulfaguanidine-linked molecules, *Egypt. J. Chem.*, 2025, **68**, 159–174, DOI: 10.21608/ejchem.2025.357091.11242.

48 F. F. Albelwi, A. Al Sheikh, M. R. Aouad, H. A. Neyaz, M. M. Khalifa, A. A. Awaji, H. E. A. Ahmed and N. Rezki, Discovery of potent anticancer tricarboxamide analogs linked to 1,2,3-triazole, promoting EGFR and VEGFR downregulation, *New J. Chem.*, 2025, **49**, 9858–9873, DOI: 10.1039/D5NJ01143D.

49 S. K. Ihmaid, A. Aljuhani, M. Alsehli, N. Rezki, A. Alawi, A. J. Aldhafiri, S. A. Salama, H. E. A. Ahmed and M. R. Aouad, Discovery of triaromatic flexible agents bearing 1,2,3-Triazole with selective and potent anti-breast cancer activity and CDK9 inhibition supported by molecular dynamics, *J. Mol. Struct.*, 2022, **1249**, 131568, DOI: 10.1016/j.molstruc.2021.131568.

50 M. Alsehli, A. Aljuhani, S. K. Ihmaid, S. M. El-Messery, D. I. A. Othman, A.-A. A. A. El-Sayed, H. E. A. Ahmed, N. Rezki and M. R. Aouad, Design and Synthesis of Benzene Homologues Tethered with 1,2,4-Triazole and 1,3,4-Thiadiazole Motifs Revealing Dual MCF-7/HepG2 Cytotoxic Activity with Prominent Selectivity via Histone Demethylase LSD1 Inhibitory Effect, *Int. J. Mol. Sci.*, 2022, **23**, 8796, DOI: 10.3390/ijms23158796.

51 H. S. Abulkhair, A bottomless well: 1,2,4-Triazoles continue to inspire scientific researchers to develop more and more anticancer molecules, *Bioorg. Med. Chem.*, 2025, **130**, 118389, DOI: 10.1016/j.bmc.2025.118389.

52 A. Musa, H. S. Abulkhair, A. Aljuhani, N. Rezki, M. A. Abdelgawad, K. Shalaby, A. H. El-Ghorab and

M. R. Aouad, Phenylpyrazolone-1,2,3-triazole Hybrids as Potent Antiviral Agents with Promising SARS-CoV-2 Main Protease Inhibition Potential, *Pharmaceuticals*, 2023, **16**, 463, DOI: 10.3390/ph16030463.

53 H. Abdelbaki, A. Djemoui, M. R. Ouahrani, M. Messaoudi, I. Ben Amor, H. Alsaeedi, D. CORNU, M. Bechelany and A. Barhoum, Synthesis of bioactive 1,4-disubstituted 1,2,3-triazole-linked Thiosemicarbazone derivatives using Cu2O microbeads catalysis for enhanced antibacterial and antioxidant activities, *J. Mol. Struct.*, 2025, **1324**, 140784, DOI: 10.1016/j.molstruc.2024.140784.

54 P. Sooknual, R. Pingaew, K. Phopin, W. Ruankham, S. Prachayasittikul, S. Ruchirawat and V. Prachayasittikul, Synthesis and neuroprotective effects of novel chalcone-triazole hybrids, *Bioorg. Chem.*, 2020, **105**, 104384, DOI: 10.1016/j.bioorg.2020.104384.

55 N. T. P. Nyoni, N. B. Ncube, M. X. Kubheka, N. P. Mkhwanazi, S. Senzani, T. Singh and M. Tukulula, Synthesis, characterization, in vitro antimycobacterial and cytotoxicity evaluation, DFT calculations, molecular docking and ADME studies of new isomeric benzimidazole-1,2,3-triazole-quinoline hybrid mixtures, *Bioorg. Chem.*, 2023, **141**, 106904, DOI: 10.1016/j.bioorg.2023.106904.

56 G. Singh, A. Majeed, R. Singh, N. George, G. Singh, S. Gupta, H. Singh, G. Kaur and J. Singh, CuAAC ensembled 1,2,3-triazole linked nanogels for targeted drug delivery: a review, *RSC Adv.*, 2023, **13**, 2912–2936, DOI: 10.1039/D2RA05592A.

57 X. Wei, M. Song, W. Li, J. Huang, G. Yang and Y. Wang, Multifunctional nanoplatforms co-delivering combinatorial dual-drug for eliminating cancer multidrug resistance, *Theranostics*, 2021, **11**, 6334–6354, DOI: 10.7150/thno.59342.

58 K. Laxmikeshav, M. Sayali, G. Devabattula, D. G. Valapil, A. Mahale, P. Sharma, J. George, R. Phanindranath, C. Godugu, O. P. Kulkarni, N. Nagesh and N. Shankaraiah, Triazolo-linked benzimidazoles as tubulin polymerization inhibitors and DNA intercalators: Design, synthesis, cytotoxicity, and docking studies, *Arch. Pharm.*, 2023, **356**, e2200449, DOI: 10.1002/ardp.202200449.

59 D. I. A. Othman, A. Hamdi, S. S. Tawfik, A. A. Elgazar and A. S. Mostafa, Identification of new benzimidazole-triazole hybrids as anticancer agents: multi-target recognition, in vitro and in silico studies, *J. Enzyme Inhib. Med. Chem.*, 2023, **38**, 1–17, DOI: 10.1080/14756366.2023.2166037.

60 O. Ommi, S. Chilvery, P. S. Dhopat, A. Sharma, H. A. Bhalerao, S. R. Dannaram, S. Nanduri, R. Sonti, C. Godugu and V. M. Yaddanapudi, Exploration of quinoxaline-benzimidazole hybrids as apoptosis-inducing agents and tubulin polymerisation inhibitors, *J. Mol. Struct.*, 2023, **1292**, 136184, DOI: 10.1016/j.molstruc.2023.136184.

61 K. J. Harkala, L. Eppakayala and T. C. Maringanti, Synthesis and biological evaluation of benzimidazole-linked 1,2,3-triazole congeners as agents, *Org. Med. Chem. Lett.*, 2014, **4**, 14, DOI: 10.1186/s13588-014-0014-x.

62 P. Pinnoju, S. Kudikala, M. Scandakashi, M. Ramesh and S. Madderla, In Vitro Antibreast Cancer and Anti-EGFR Studies of Some Novel Benzimidazole-Piperazine Containing 1,2,3-Triazoles, *Russ. J. Bioorg. Chem.*, 2024, **50**, 1724–1734, DOI: 10.1134/S106816202405025X.

63 B. Ma, Q. Li, J. Zhang, Y. Mi, W. Tan and Z. Guo, Improvement of the Antioxidant and Antitumor Activities of Benzimidazole-Chitosan Quaternary Ammonium Salt on Drug Delivery Nanogels, *Mar. Drugs*, 2024, **22**, 40, DOI: 10.3390/md22010040.

64 G. Pastuch-Gawołek, J. Szreder, M. Domińska, M. Pielok, P. Cichy and M. Grymel, A Small Sugar Molecule with Huge Potential in Targeted Cancer Therapy, *Pharmaceutics*, 2023, **15**, 913, DOI: 10.3390/pharmaceutics15030913.

65 Z. Wen, Azido- and Triazolyl-Modified Nucleoside/tide Analogues: Chemistry, Fluorescent Properties, and Anticancer Activities, *PhD thesis*, Florida International University, 2018, p. 3789, DOI: 10.25148/etd.FIDC006844.

66 A. M. Srour, M. N. El-Bayaa, A. Temirak, A. L. Alanzy, H. M. Awad, A. Saleh, M. G. Saleh and W. A. El-Sayed, New benzimidazole-triazole glycoconjugates as anti-cancer agents and EGFR inhibitors, *Sci. Rep.*, 2025, **15**, 25514, DOI: 10.1038/s41598-025-96675-3.

67 N. Sridhar Goud, V. Pooladanda, K. Muni Chandra, P. S. Lakshmi Soukya, R. Alvala, P. Kumar, C. Nagaraj, R. Dawn Bharath, I. A. Qureshi, C. Godugu and M. Alvala, Novel benzimidazole-triazole hybrids as apoptosis inducing agents in lung cancer: Design, synthesis, 18F-radiolabeling & galectin-1 inhibition studies, *Bioorg. Chem.*, 2020, **102**, 104125, DOI: 10.1016/j.bioorg.2020.104125.

68 H. E. A. Ahmed, A. Amer, S. A. Senior, S. Ihmaid, M. Almalghrabi, A.-M. El Massry, S. Ahmed, A. Musa, M. A. Almikhlafi, S. A. Salama and A. A. Elhenawy, Extensive Study of DFT-Quantum Calculations Based QSAR Modeling of Fused 1,2,4-Triazine Derivatives Revealed Potent CYP1A1 Inhibitors, *J. Comput. Biophys. Chem.*, 2022, **21**, 741–758, DOI: 10.1142/S2737416522300036.

69 M. T. Khayat, H. E. A. Ahmed, A. M. Omar, Y. A. Muhammad, K. A. Mohammad, A. M. Malebari, A. N. Khayyat, A. H. Halawa, H. S. Abulkhair, A. A. Al-Karmalawy, M. Almaghrabi, M. Alharbi, A. S. Aljahdali and A. M. El-Agrody, A novel class of phenylpyrazolone-sulphonamides rigid synthetic anticancer molecules selectively inhibit the isoform IX of carbonic anhydrases guided by molecular docking and orbital analyses, *J. Biomol. Struct. Dyn.*, 2023, **41**, 15243–15261, DOI: 10.1080/07391102.2023.2188957.

70 A. M. Omar, S. Ihmaid, E. S. E. Habib, S. S. Althagfan, S. Ahmed, H. S. Abulkhair and H. E. A. Ahmed, The rational design, synthesis, and antimicrobial investigation of 2-Amino-4-Methylthiazole analogues inhibitors of GlcN-6-P synthase, *Bioorg. Chem.*, 2020, **99**, 103781, DOI: 10.1016/j.bioorg.2020.103781.

71 A. M. Malebari, H. E. A. Ahmed, S. K. Ihmaid, A. M. Omar, Y. A. Muhammad, S. S. Althagfan, N. Aljuhani, A. A. A. A. El-Sayed, A. H. Halawa, H. M. El-Tahir, S. A. Turkistani, M. Almaghrabi, A. K. B. Aljohani, A. M. El-Agrody and H. S. Abulkhair, Exploring the dual effect of novel 1,4-diarylpyranopyrazoles as antiviral and anti-inflammatory for the management of SARS-CoV-2 and

associated inflammatory symptoms, *Bioorg. Chem.*, 2023, **130**, 106255, DOI: 10.1016/j.bioorg.2022.106255.

72 M. C. Ocaña, B. Martínez-Poveda, A. R. Quesada and M. Á. Medina, Glucose Favors Lipid Anabolic Metabolism in the Invasive Breast Cancer Cell Line MDA-MB-231, *Biology*, 2020, **9**, 16, DOI: 10.3390/biology9010016.

73 C. Morresi, M. Vasarri, L. Bellachioma, G. Ferretti, D. Degl′Innocenti and T. Bacchetti, Glucose Uptake and Oxidative Stress in Caco-2 Cells: Health Benefits from Posidonia oceanica (L.) Delile, *Mar. Drugs*, 2022, **20**, 457, DOI: 10.3390/md20070457.

74 B. Almohaywi, M. H. Elkomy, M. A. M. Ali, A. K. B. Aljohani, M. S. Abdulrahman, M. M. Elsebaie, A. M. Alhammad, K. A. Aytah, S. M. Alshehri, E. O. Alharbi, R. R. Alharbi and H. E. A. Ahmed, Development of carboximidamide small molecule nanogels as potent antimicrobial functional drug delivery systems, *RSC Adv.*, 2025, **15**, 35941–35960, DOI: 10.1039/D5RA05150A.

75 J. Nauta, in *Standard Statistical Methods for Immunogenicity Data*, 2020, pp. 23–49, DOI: 10.1007/978-3-030-37693-2_3.

76 B. Srinivasan and M. D. Lloyd, Quantitation and Error Measurements in Dose–Response Curves, *J. Med. Chem.*, 2025, **68**, 2052–2056, DOI: 10.1021/acs.jmedchem.5c00131.

77 F. Kappenberg, J. C. Duda, L. Schürmeyer, O. Gül, T. Brecklinghaus, J. G. Hengstler, K. Schorning and J. Rahnenführer, Guidance for statistical design and analysis of toxicological dose–response experiments, based on a comprehensive literature review, *Arch. Toxicol.*, 2023, **97**, 2741–2761, DOI: 10.1007/s00204-023-03561-w.

78 M. Dai, C. Zhang, A. Ali, X. Hong, J. Tian, C. Lo, N. Fils-Aimé, S. A. Burgos, S. Ali and J.-J. Lebrun, CDK4 regulates cancer stemness and is a novel therapeutic target for triple-negative breast cancer, *Sci. Rep.*, 2016, **6**, 35383, DOI: 10.1038/srep35383.

79 X. Jia, Y. Zhao, Q. Li, X. Lu, X. Wang, H. Wang, Z. Shi, Y. Xu, B. Huang, F. Huang and Y. Wang, Targeted Inhibition of p21 Promotes the Growth of Breast Cancer Cells and Impairs the Tumor-Killing Effect of the Vaccinia Virus, *J. Breast Cancer*, 2024, **27**, 293, DOI: 10.4048/jbc.2024.0063.

80 F. F. Al-blewi, M. A. Almehmadi, M. R. Aouad, S. K. Bardaweel, P. K. Sahu, M. Messali, N. Rezki and E. S. H. El Ashry, Design, synthesis, ADME prediction and pharmacological evaluation of novel benzimidazole-1,2,3-triazole-sulfonamide hybrids as antimicrobial and antiproliferative agents, *Chem. Cent. J.*, 2018, **12**, 110, DOI: 10.1186/s13065-018-0479-1.

81 M. R. Aouad, M. A. Almehmadi, N. Rezki, F. F. Al-blewi, M. Messali and I. Ali, Design, click synthesis, anticancer screening and docking studies of novel benzothiazole-1,2,3-triazoles appended with some bioactive benzofused heterocycles, *J. Mol. Struct.*, 2019, **1188**, 153–164, DOI: 10.1016/j.molstruc.2019.04.005.

82 S. M. Al-Mousawi, M. S. Moustafa and M. H. Elnagdi, On the reaction of phenacylmalononitrile with hydrazines: A new route to pyrazolo[3,4-c]pyridazine, isoxazolo[5,4-c]pyridazine and pyrimido[4,5-c]pyridazine, *J. Saudi Chem. Soc.*, 2011, **15**, 309–312, DOI: 10.1016/j.jscs.2011.07.011.

83 R. Zhong, S. Talebian, B. B. Mendes, G. Wallace, R. Langer, J. Conde and J. Shi, Hydrogels for RNA delivery, *Nat. Mater.*, 2023, **22**, 818–831, DOI: 10.1038/s41563-023-01472-w.

84 D. M. L. Morgan, Tetrazolium (MTT) Assay for Cellular Viability and Activity, *Methods Mol. Biol.*, 1998, **79**, 179–183, DOI: 10.1385/0-89603-448-8:179.

85 F. G. Abdulrahman, H. S. Abulkhair, R. A. Zidan, A. I. Alwakeel, A. A. Al-Karmalawy and E. M. Husseiny, Novel benzochromenes: design, synthesis, cytotoxicity, molecular docking and mechanistic investigations, *Future Med. Chem.*, 2024, **16**, 105–123, DOI: 10.4155/fmc-2023-0198.

86 S. Ihmaid, H. E. A. Ahmed, A. Al-Sheikh Ali, Y. E. Sherif, H. M. Tarazi, S. M. Riyadh, M. F. Zayed, H. S. Abulkhair and H. S. Rateb, Rational design, synthesis, pharmacophore modeling, and docking studies for identification of novel potent DNA-PK inhibitors, *Bioorg. Chem.*, 2017, **72**, 234–247, DOI: 10.1016/j.bioorg.2017.04.014.

87 G. M. Morris, D. S. Goodsell, R. S. Halliday, R. Huey, W. E. Hart, R. K. Belew and A. J. Olson, Automated docking using a Lamarckian genetic algorithm and an empirical binding free energy function, *J. Comput. Chem.*, 1998, **19**, 1639–1662, DOI: 10.1002/(SICI)1096-987X(19981115)19:14<1639::AID-JCC10>3.0.CO;2-B.

88 S. Dallakyan and A. J. Olson, in *Small-Molecule Library Screening by Docking with PyRx*, 2015, pp. 243–250, DOI: 10.1007/978-1-4939-2269-7_19.

89 A. D. Becke, Density-functional exchange-energy approximation with correct asymptotic behavior, *Phys. Rev. A*, 1988, **38**, 3098–3100, DOI: 10.1103/PhysRevA.38.3098.